Institut Pprime
Research in physics and engineering

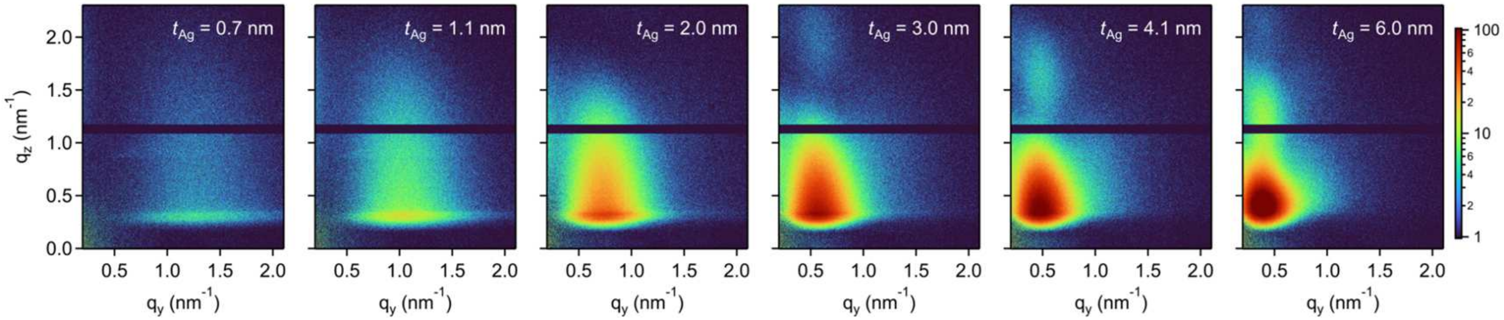

Grazing-Incidence SAXS: Basic Principles and Applications

David BABONNEAU

Université de Poitiers, ISAE-ENSMA, CNRS, Institut Pprime, Poitiers, France

david.babonneau@univ-poitiers.fr

Institut Pprime

Introduction

GISAXS combines the accessible length scales of small-angle X-ray scattering (**TSAXS**) and the surface sensitivity of grazing incidence X-ray techniques (GID, XRR, etc.)

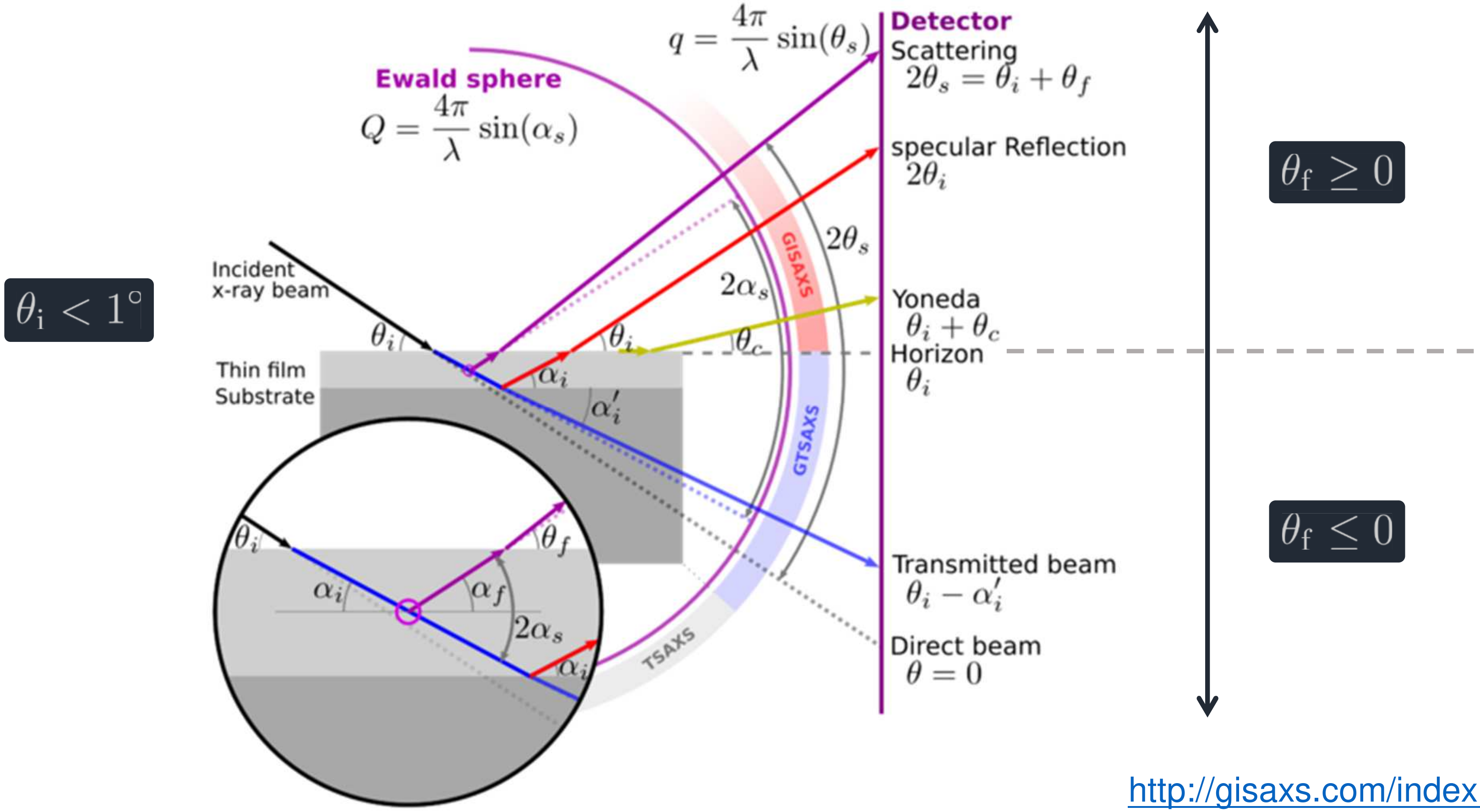

http://gisaxs.com/index.php/GISAXS

Introduction

A look back at the origins of GISAXS

J. Appl. Cryst. (1989). **22**, 528–532

Grazing-Incidence Small-Angle X-ray Scattering: New Tool for Studying Thin Film Growth

By Joanne R. Levine, J. B. Cohen, Y. W. Chung and P. Georgopoulos

Department of Materials Science and Engineering, The Technological Institute, Northwestern University, Evanston, Illinois 60208, USA

Abstract

Grazing-incidence small-angle X-ray scattering (GISAXS) is introduced as a method of studying discontinuous thin films. In this method, the incident beam is totally externally reflected from the substrate followed by small-angle scattering of the refracted beam by the thin film. The experiment described establishes the ability of GISAXS to provide size information for islands formed in the initial stages of thin film growth. The data presented are for gold films of 7 and 15 Å average thicknesses on Corning 7059 glass substrates. The advantages of this technique are that it is non-destructive, can be done *in situ*, provides excellent sampling statistics, does not necessarily require a synchrotron source, and is not limited to thin or conducting substrates.

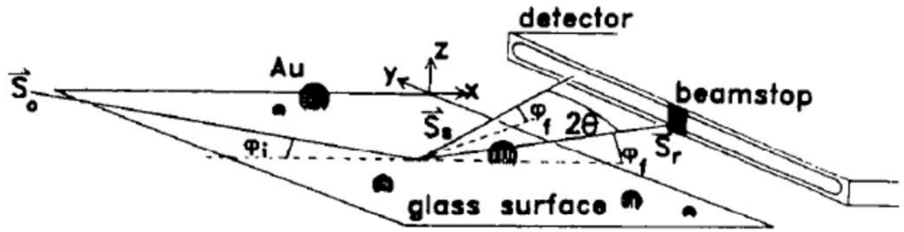

Fig. 1. Schematic diagram of GISAXS alignment.

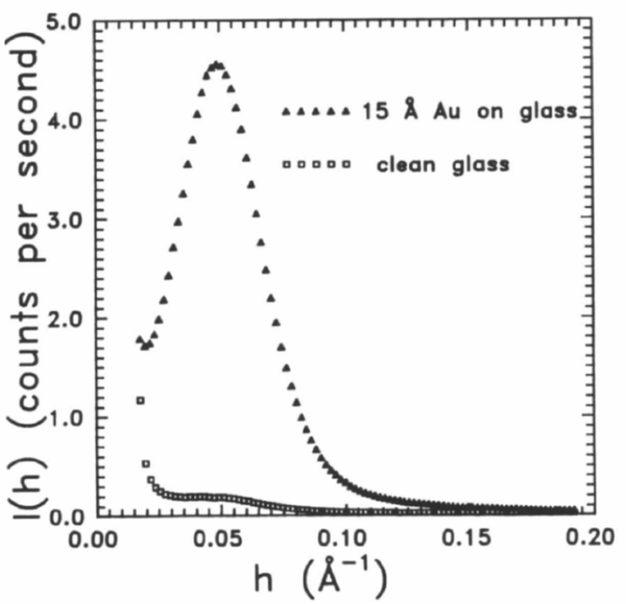

Fig. 3. Scattered intensity from clean Corning 7059 glass and from 15 Å Au on glass.

- Rotating anode ($\lambda = 0.154$ nm)
- Linear position-sensitive detector
- Grazing incidence and exit angles
  $\rightarrow \varphi_i = \varphi_f = 0.229°$

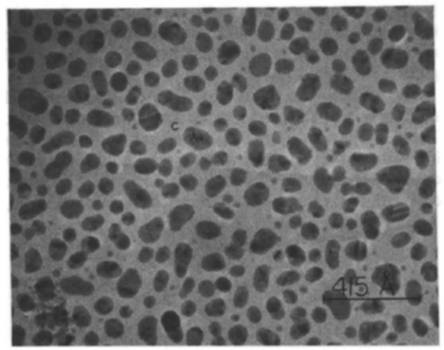

Fig. 2. TEM micrograph of 15 Å Au film.

Introduction

Brief overview of bibliographic data (1989–2024)

Web of Science^{TM} database

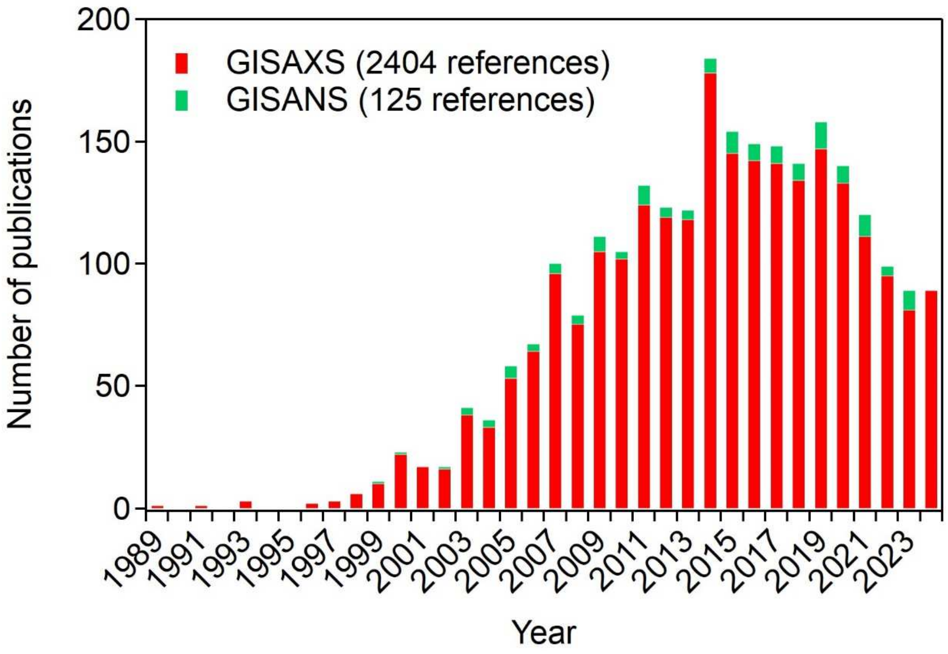

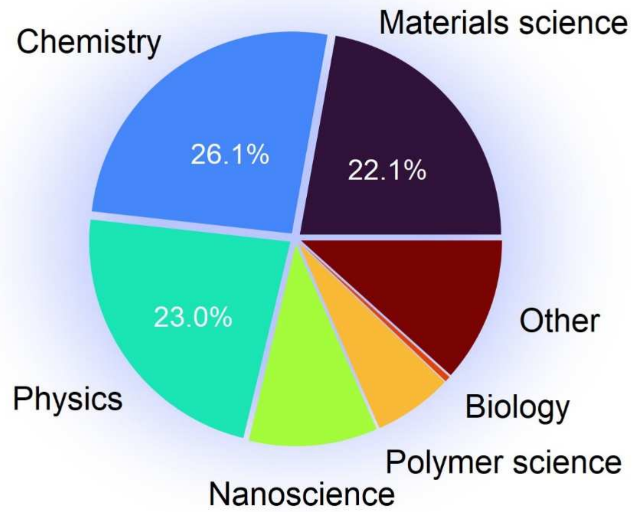

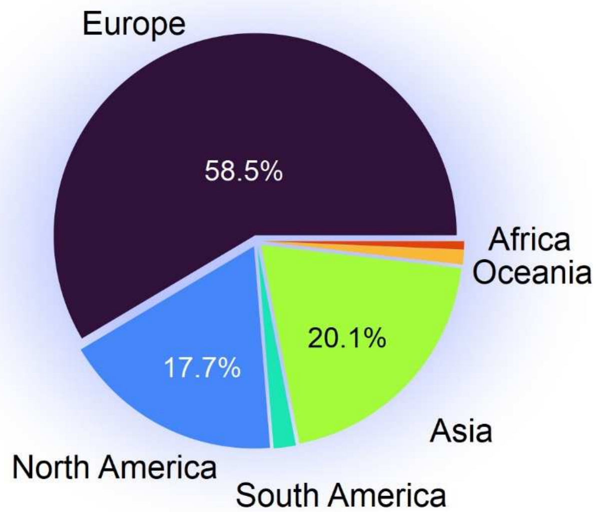

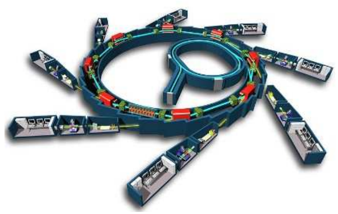

> 75% synchrotron

Why using grazing incidence conditions ?

Limitations of transmission SAXS at normal incidence

$$I = I_0 \exp\left(-\frac{z}{z_{1/e}}\right)$$

- Small size of the incident beam limits the volume irradiated
- Absorption causes a strong decrease of the signal-to-noise ratio

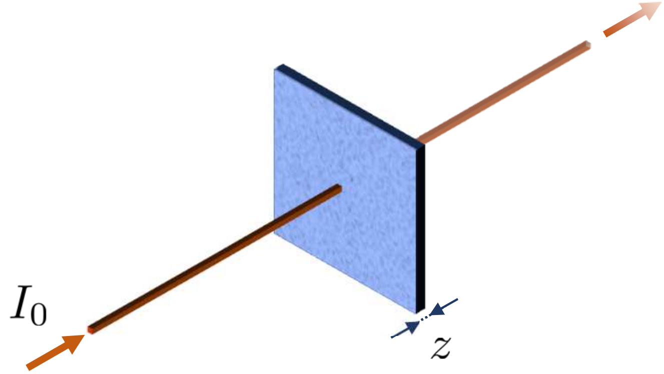

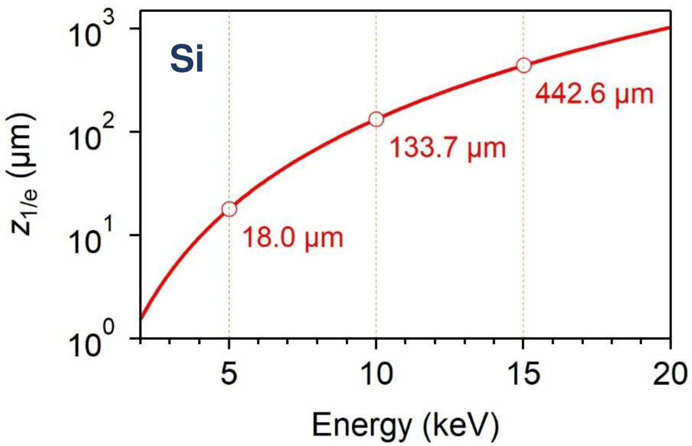

Why using grazing incidence conditions ?

Limitations of transmission SAXS at normal incidence

- Small size of the incident beam limits the volume irradiated
- Absorption causes a strong decrease of the signal-to-noise ratio
- $q_z \approx 0$
  - ✓ In-plane information only

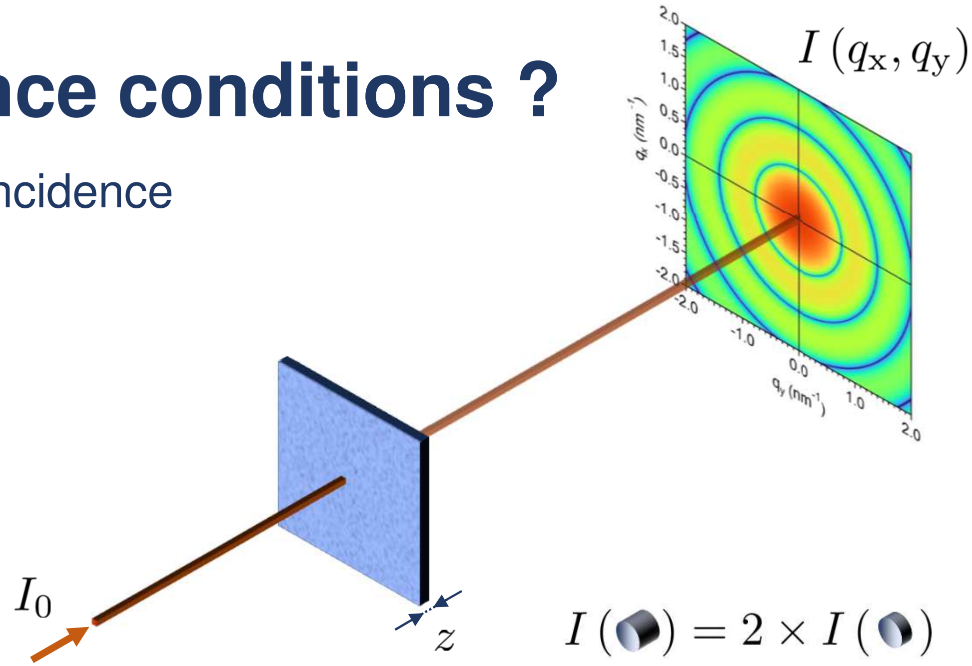

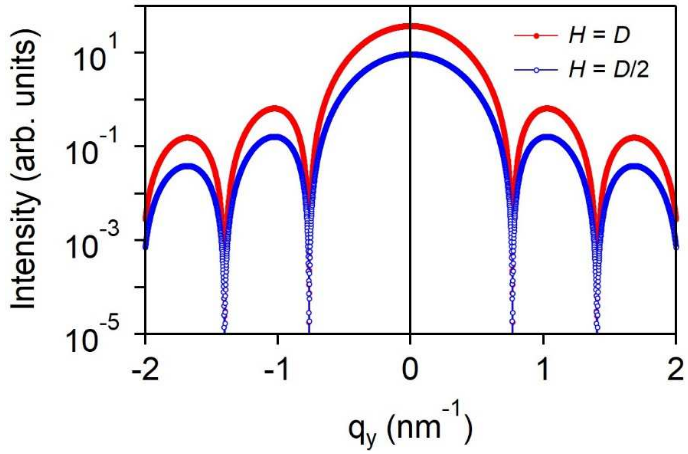

Cylinders

($D = 10$ nm)

Why using grazing incidence conditions ?

Limitations of transmission SAXS at normal incidence

- Small size of the incident beam limits the volume irradiated
- Absorption causes a strong decrease of the signal-to-noise ratio
- $q_z \approx 0$
  - ✓ In-plane information only
  - ✓ SAXS patterns are centrosymmetric

$$I\left(q_{\mathrm{x}}, q_{\mathrm{y}}\right) = I\left(-q_{\mathrm{x}}, -q_{\mathrm{y}}\right)$$

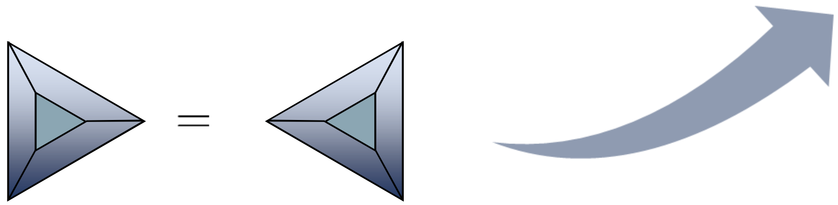

6-fold symmetry !

Truncated tetrahedron

($D = 20$ nm, $H = 15.8$ nm, $\gamma = 70^{\circ}$)

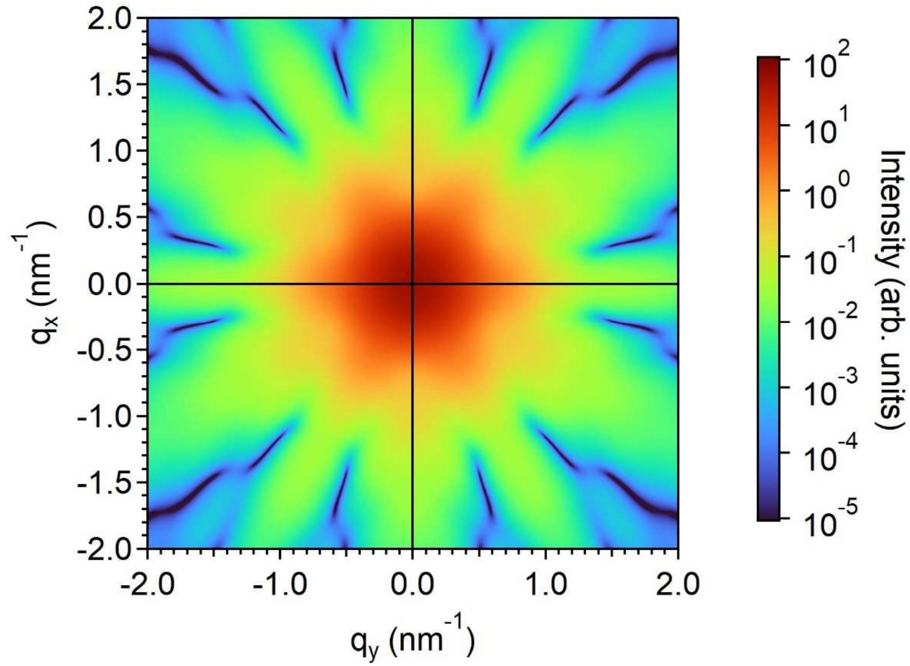

Why using grazing incidence conditions ?

Advantages and added values of GISAXS ($\alpha_i < 1^\circ$)

- Increased footprint of the primary beam at the sample surface
- Reduced depth of penetration (typically a few nanometers below α_c)

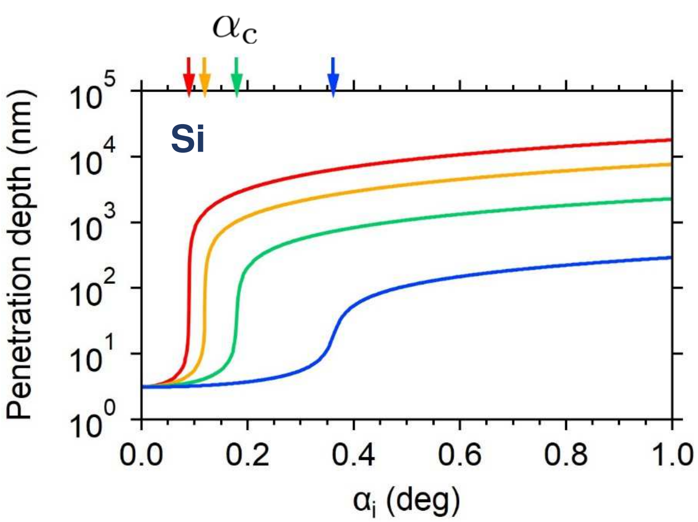

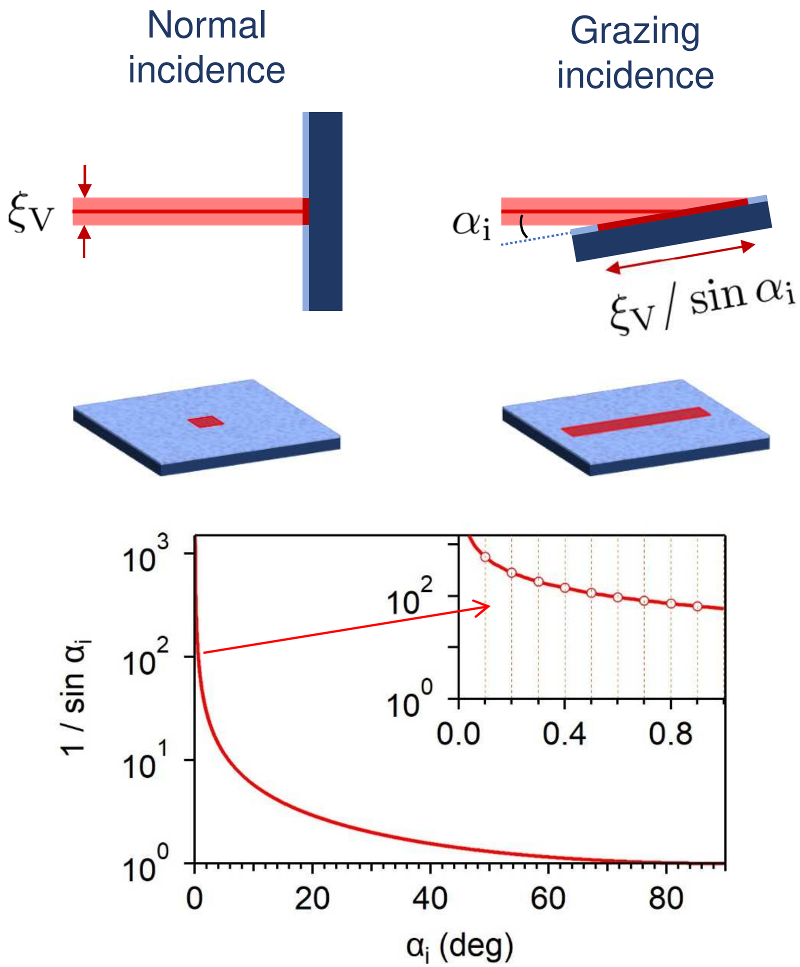

Why using grazing incidence conditions ?

Advantages and added values of GISAXS ($\alpha_i < 1^{\circ}$)

- Increased footprint of the primary beam at the sample surface
- Reduced depth of penetration (typically a few nanometers below α_c)
- Enhancement of surface sensitivity

$$I_t(z, \alpha_i) = |t_{0,1}(\alpha_i)|^2 \exp\left(-\frac{z}{z_{1/e}}\right)$$

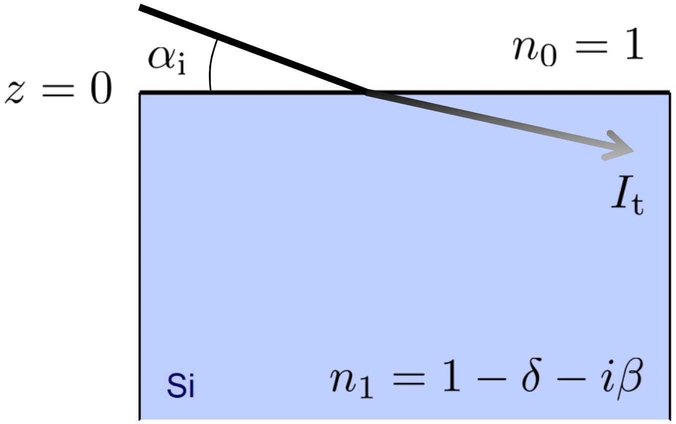

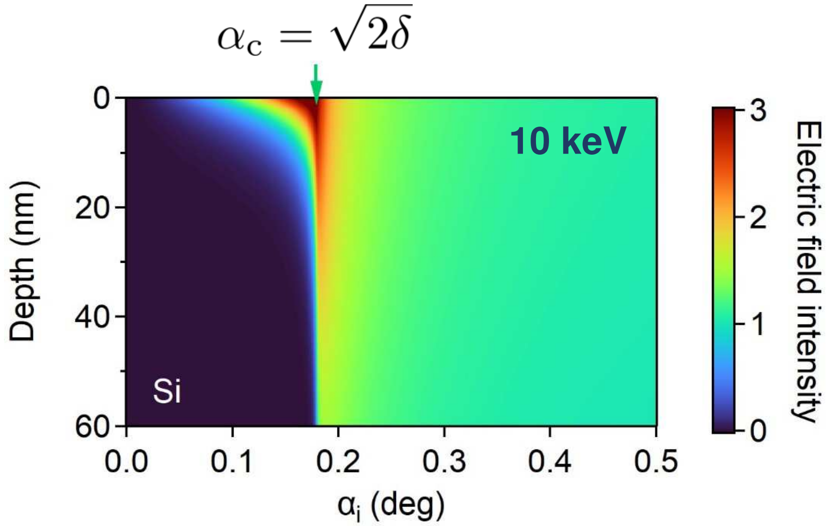

Why using grazing incidence conditions ?

Advantages and added values of GISAXS ($\alpha_i < 1^\circ$)

- Increased footprint of the primary beam at the sample surface
- Reduced depth of penetration (typically a few nanometers below α_c)
- Enhancement of surface sensitivity

$$I_t(z, \alpha_i) = |t_{0,1}(\alpha_i)|^2 \exp\left(-\frac{z}{z_{1/e}}\right)$$

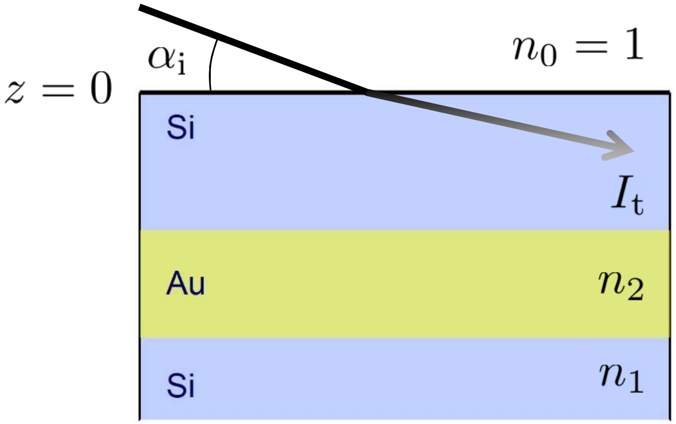

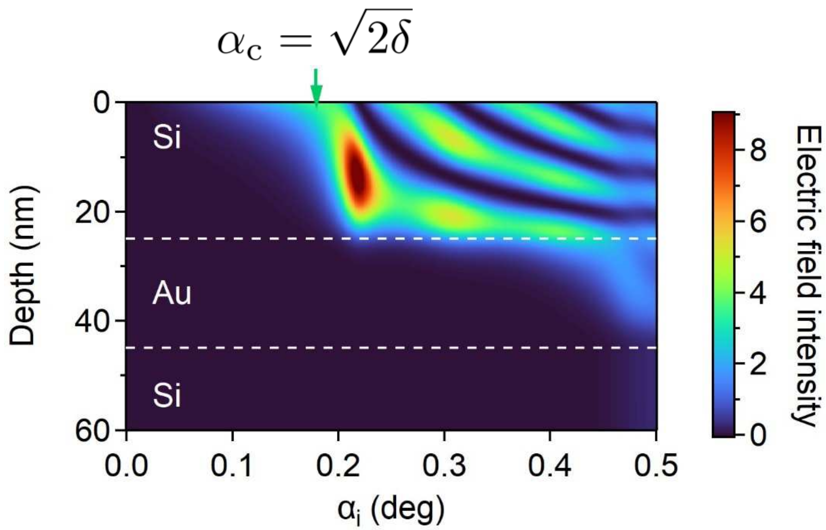

In-depth distribution of electric field intensity can be varied in a controlled way, enabling enhancement of the scattering from **supported** or **buried** nanostructures

Why using grazing incidence conditions ?

Advantages and added values of GISAXS ($\alpha_i < 1°$)

- Increased footprint of the primary beam at the sample surface
- Reduced depth of penetration (typically a few nanometers below α_c)
- Enhancement of surface sensitivity
- Scattering vector

$$\vec{q} = \frac{2\pi}{\lambda} \mathcal{Q}_z(\varphi) \begin{bmatrix} \cos(2\theta_f)\cos(\alpha_f) - \cos(\alpha_i) \\ -\sin(2\theta_f)\cos(\alpha_f) \\ \sin(\alpha_f) + \sin(\alpha_i) \end{bmatrix}$$

✓ In-plane and out-of-plane information are made accessible

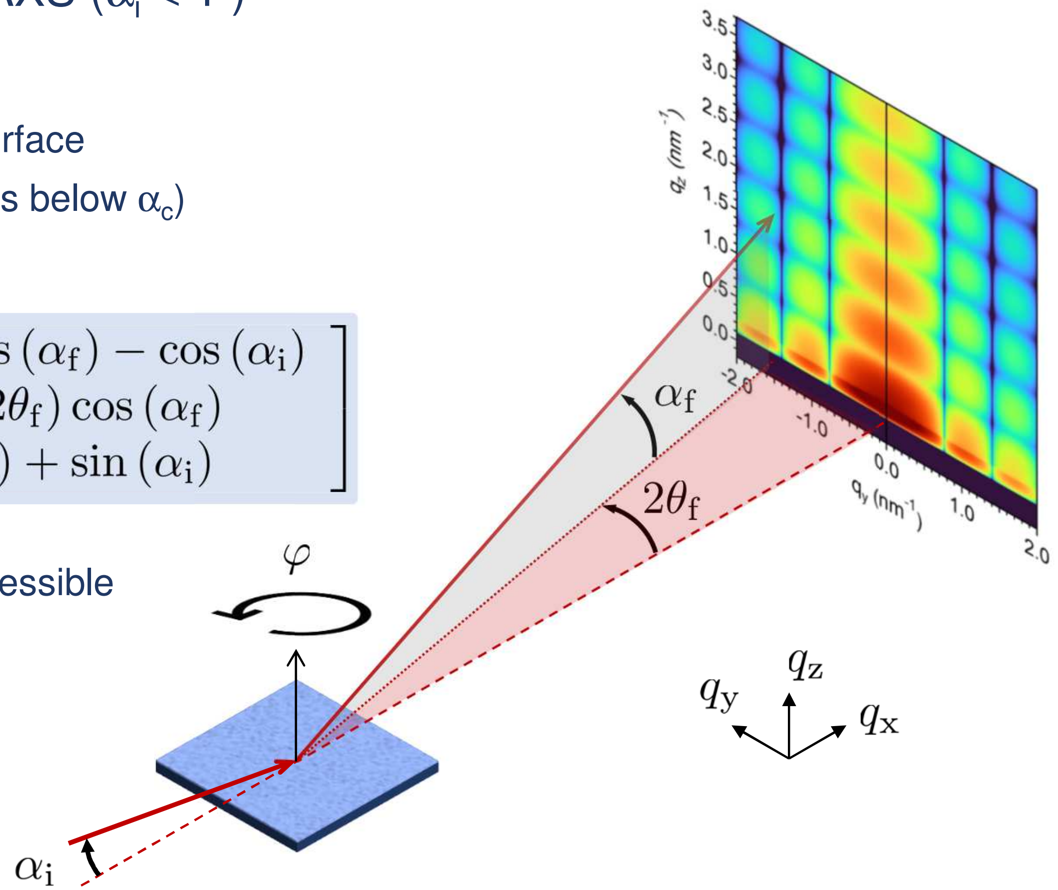

Why using grazing incidence conditions ?

Advantages and added values of GISAXS

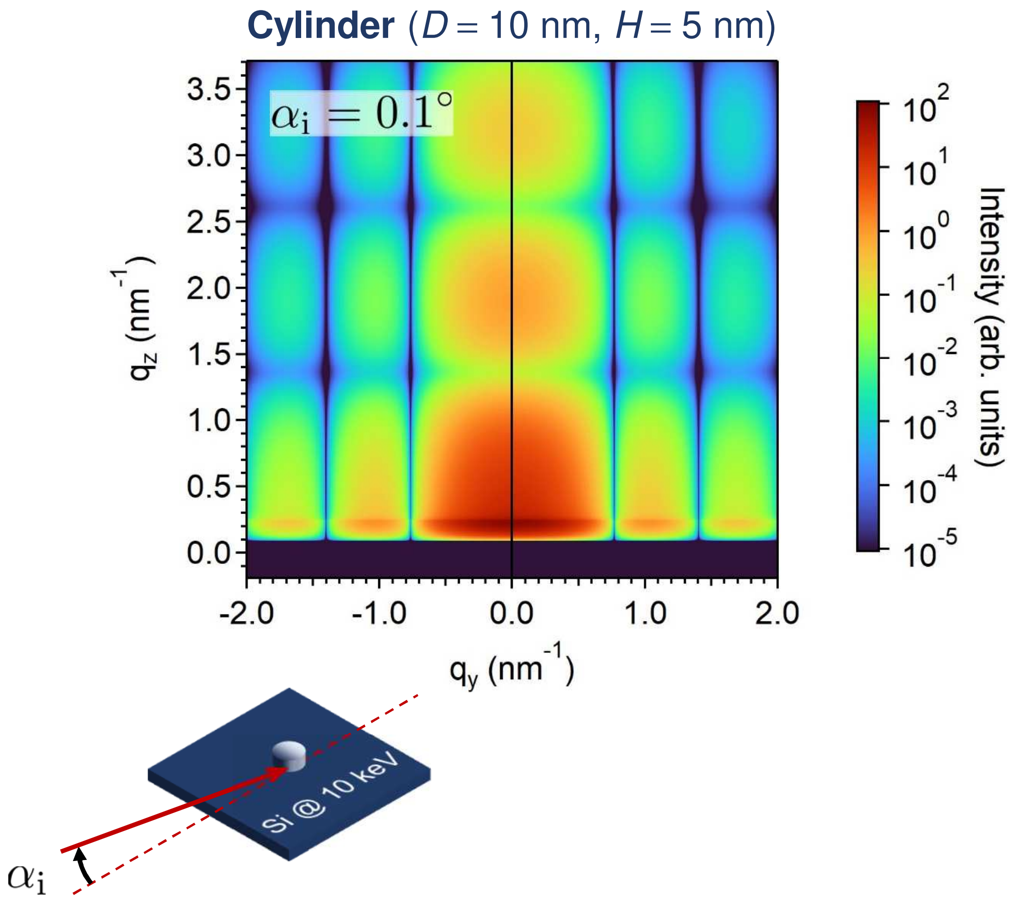

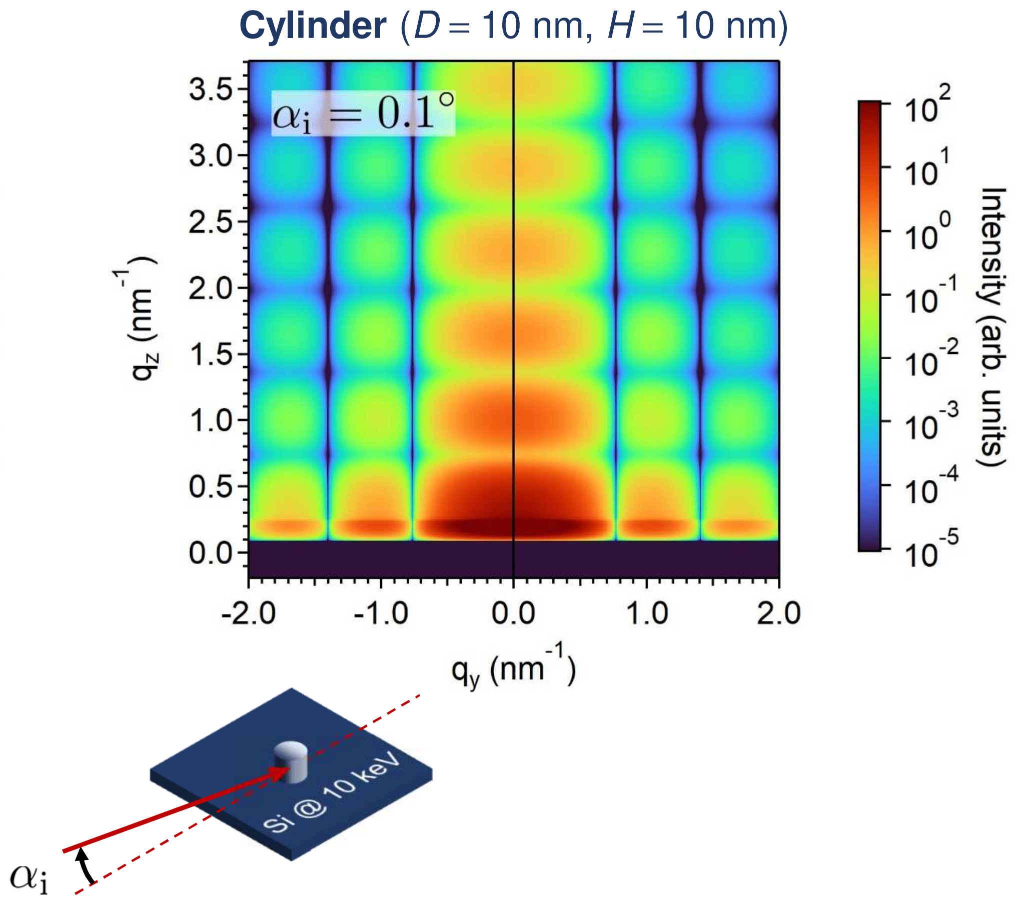

Why using grazing incidence conditions ?

Advantages and added values of GISAXS ($\alpha_i < 1^\circ$)

- Increased footprint of the primary beam at the sample surface
- Reduced depth of penetration (typically a few nanometers below α_c)
- Enhancement of surface sensitivity
- Scattering vector

$$\vec{q} = \frac{2\pi}{\lambda} \mathcal{Q}_z(\varphi) \begin{bmatrix} \cos(2\theta_f)\cos(\alpha_f) - \cos(\alpha_i) \\ -\sin(2\theta_f)\cos(\alpha_f) \\ \sin(\alpha_f) + \sin(\alpha_i) \end{bmatrix}$$

✓ In-plane and out-of-plane information are made accessible

✓ Full 3D reciprocal space mapping by changing φ (±180°)

✓ $q_z \neq 0 \Rightarrow I(q_x, q_y, q_z) \neq I(-q_x, -q_y, q_z)$

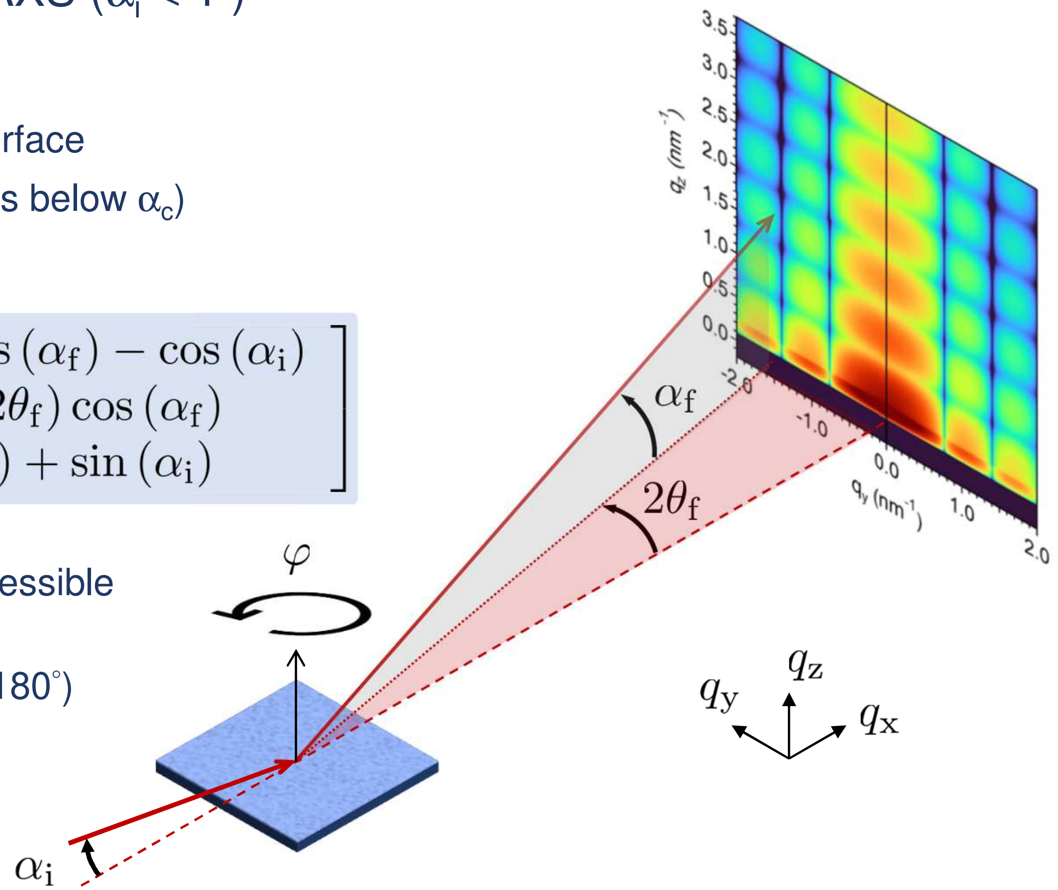

Why using grazing incidence conditions ?

Advantages and added values of GISAXS

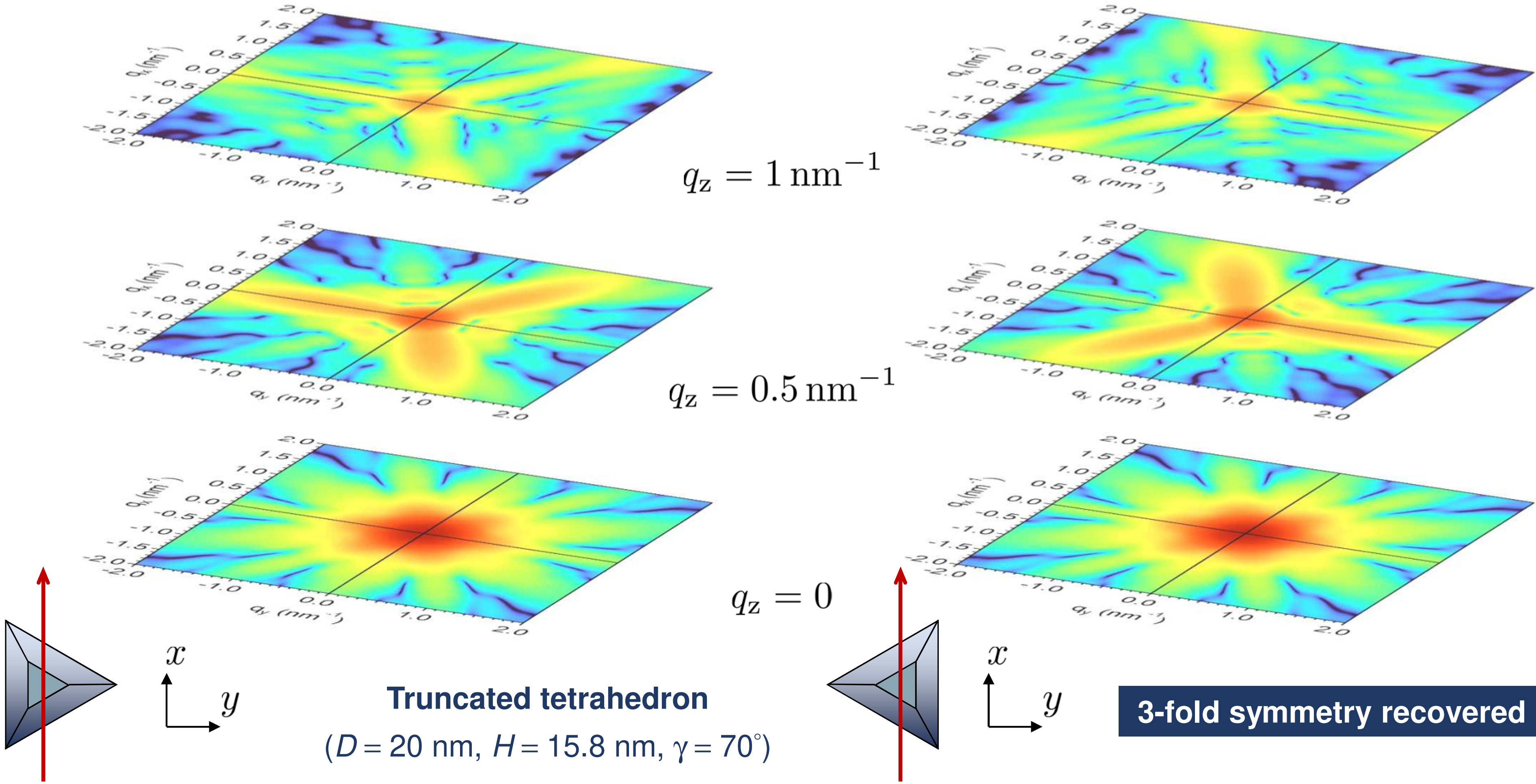

Truncated tetrahedron
($D = 20$ nm, $H = 15.8$ nm, $\gamma = 70^{\circ}$)

3-fold symmetry recovered !

Why using grazing incidence conditions ?

Advantages and added values of GISAXS

$$q_\mathrm{x} = \frac{2\pi}{\lambda}\left[\cos\left(2\theta_\mathrm{f}\right)\cos\left(\alpha_\mathrm{f}\right) - \cos\left(\alpha_\mathrm{i}\right)\right] \approx 0\ldots \text{ but } \neq 0\,!$$

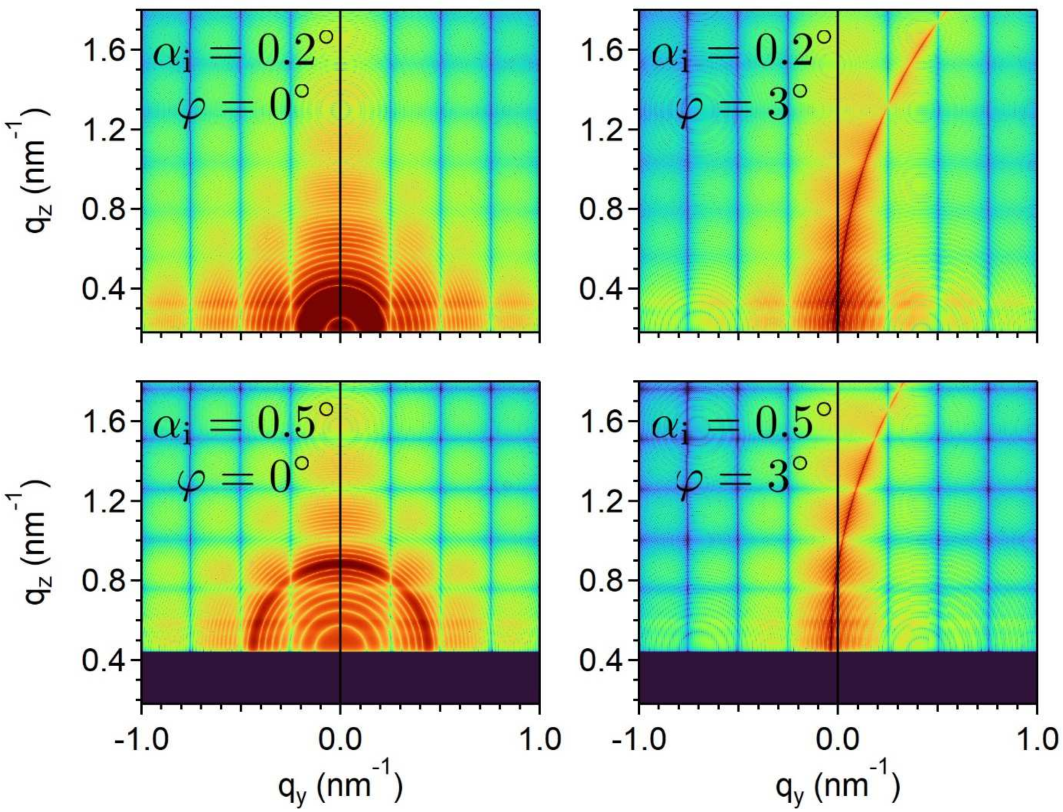

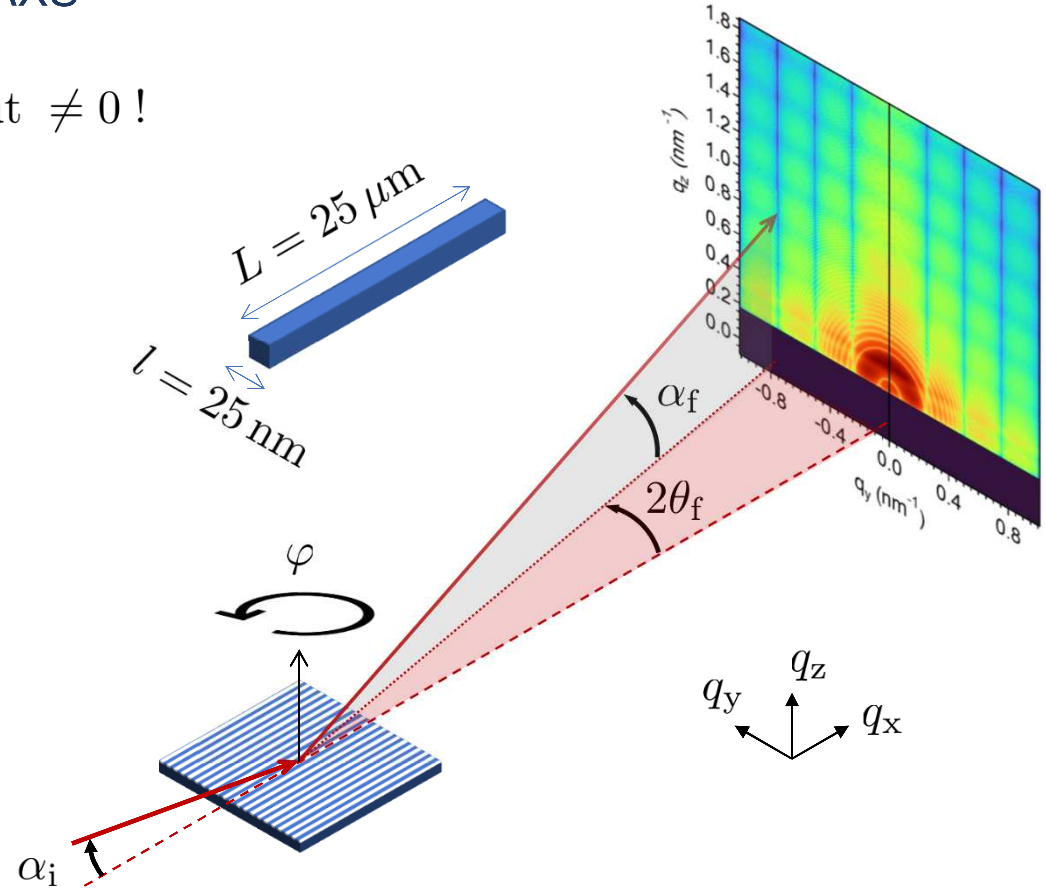

GISAXS: some points of vigilance

Influence of the angle of incidence

$$q_z = \frac{2\pi}{\lambda}\left[\sin(\alpha_f) + \sin(\alpha_i)\right] \qquad \alpha_f \geq 0 \Rightarrow q_z \geq \frac{2\pi}{\lambda}\sin(\alpha_i)$$

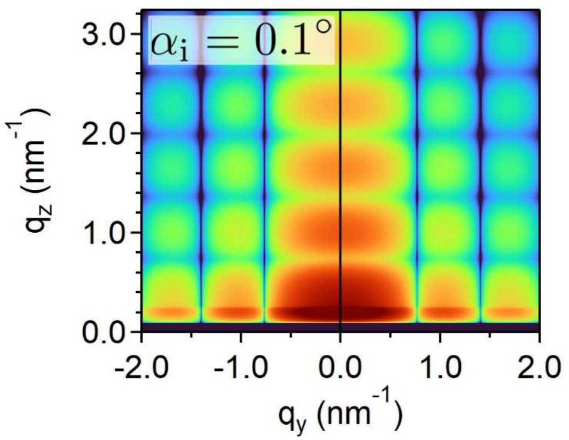

Ag cylinder

($D = 10$ nm, $H = 10$ nm)

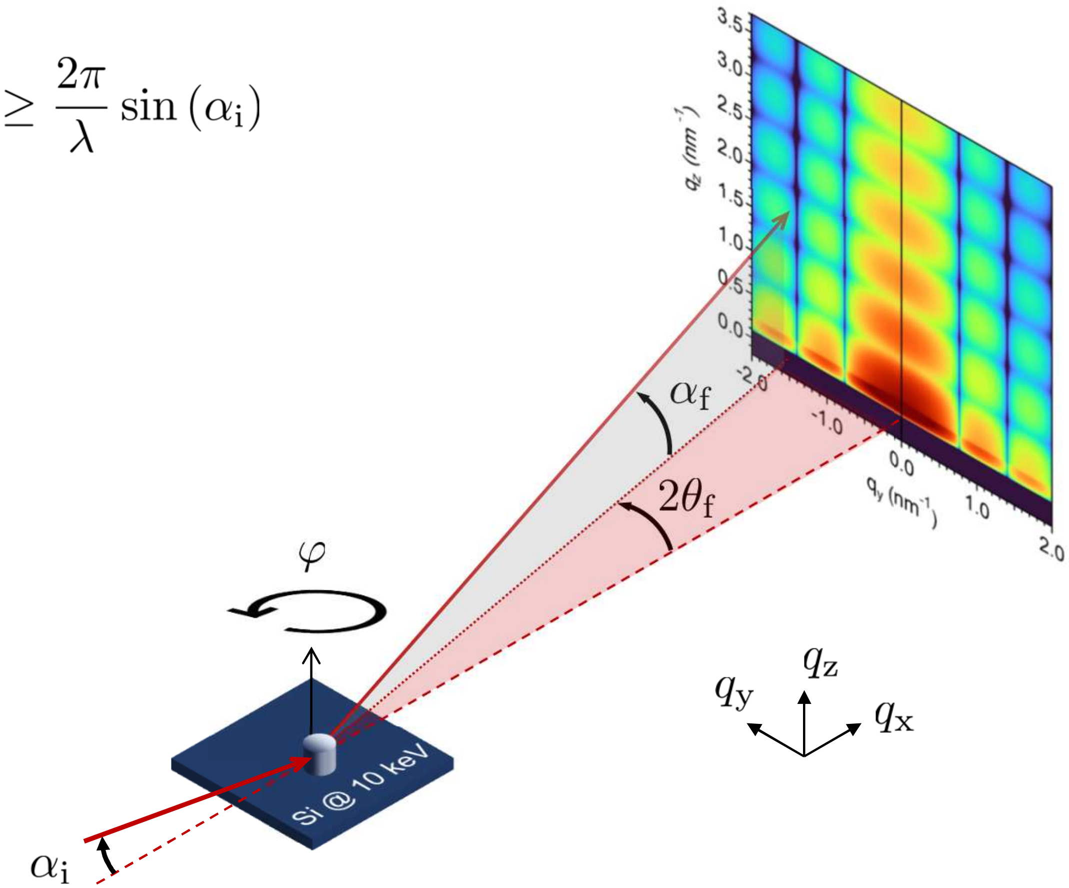

GISAXS: some points of vigilance

Influence of the angle of incidence

$$q_z = \frac{2\pi}{\lambda}\left[\sin(\alpha_f) + \sin(\alpha_i)\right] \qquad \alpha_f \geq 0 \Rightarrow q_z \geq \frac{2\pi}{\lambda}\sin(\alpha_i)$$

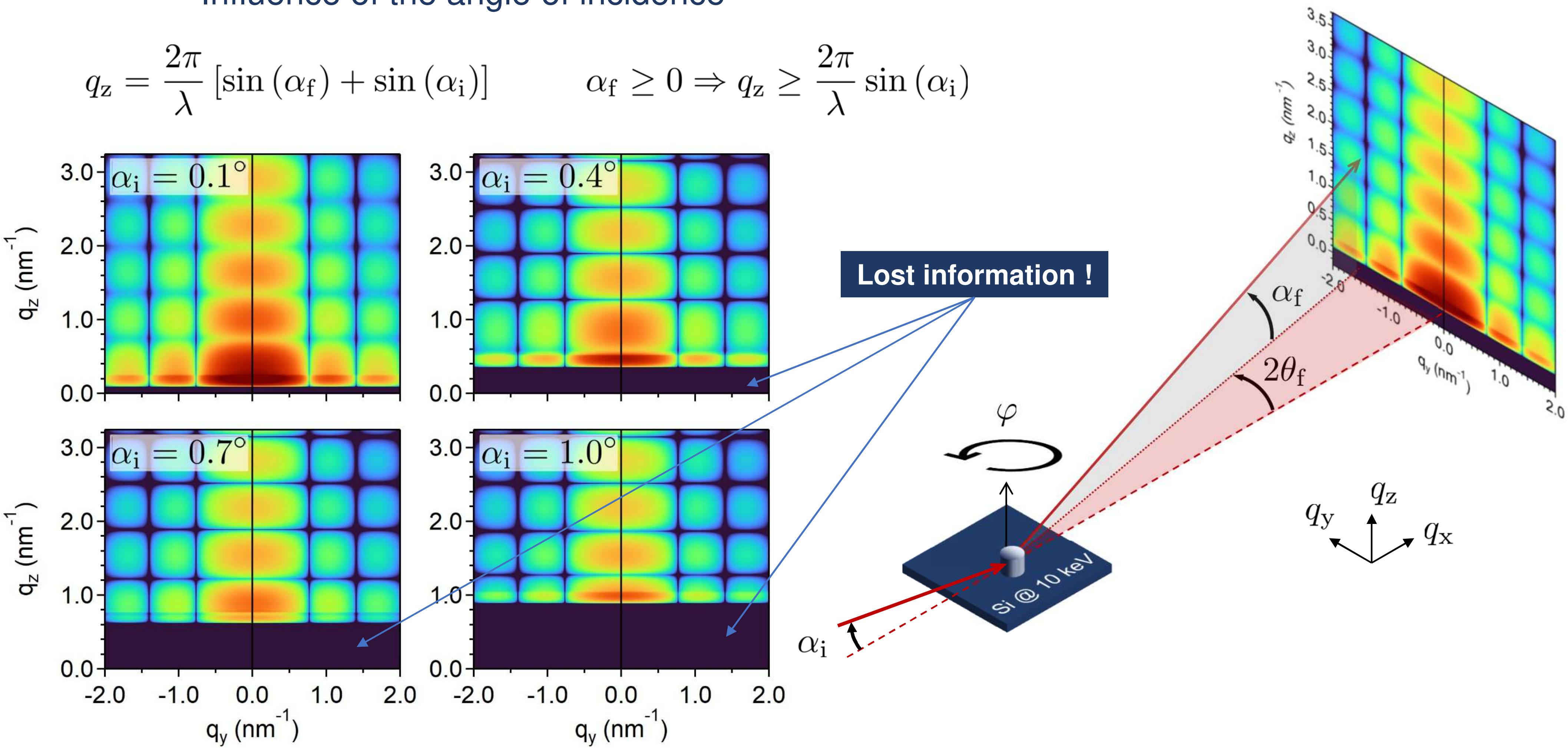

GISAXS: some points of vigilance

Influence of the sample length

$$q_z = \frac{2\pi}{\lambda}\left[\sin\left(\alpha_f\right) + \sin\left(\alpha_i\right)\right]$$

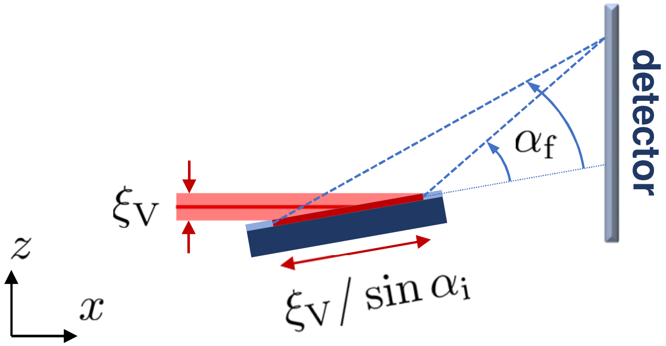

Reference ("point-like" sample) | "Small" footprint ($l = 10$ mm) | "Large" footprint ($l = 50$ mm)

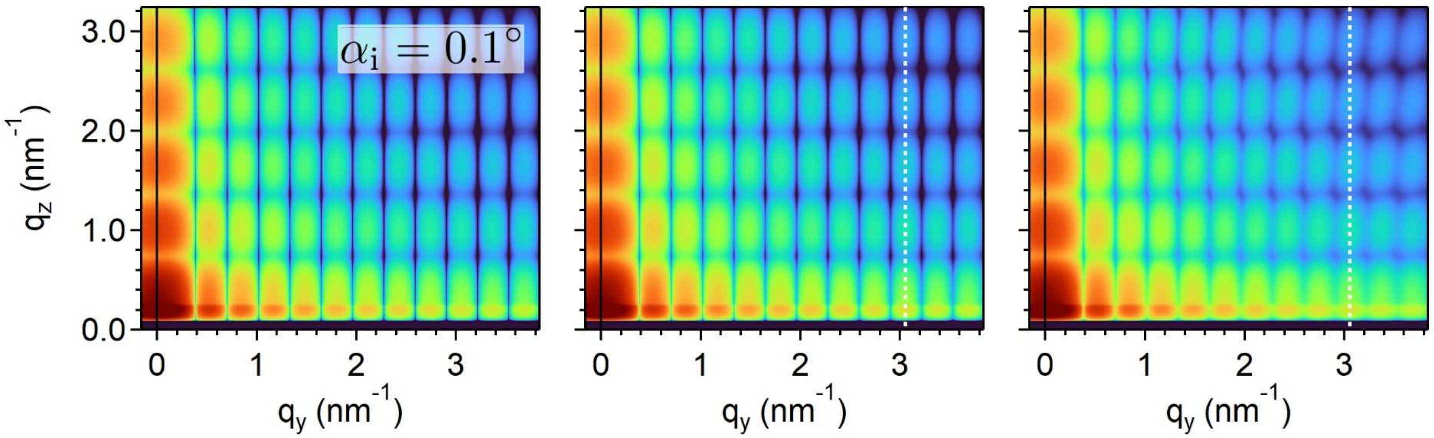

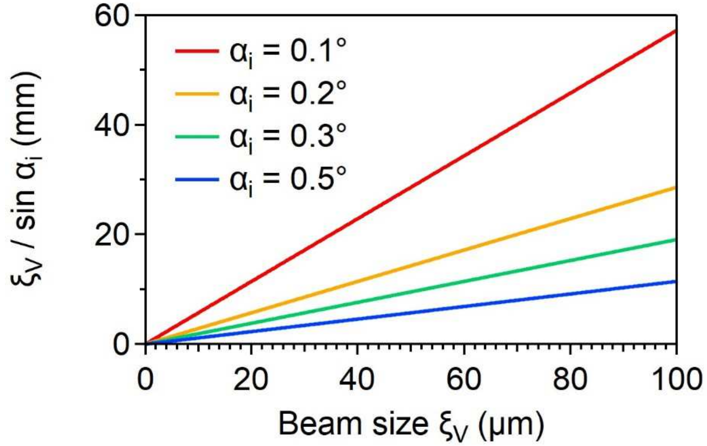

Ag cylinder @ 10 keV

($D = 20$ nm, $H = 10$ nm)

Footprint correction needed !

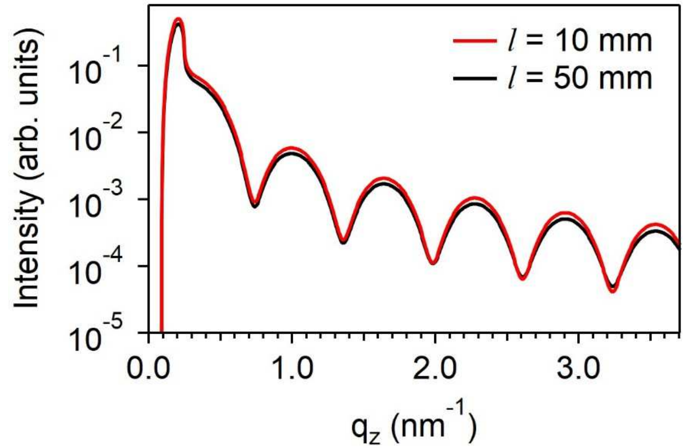

GISAXS: some points of vigilance

Influence of the sample curvature

$$q_z = \frac{2\pi}{\lambda}\left[\sin\left(\alpha_f\right) + \sin\left(\alpha_i\right)\right]$$

- Convex

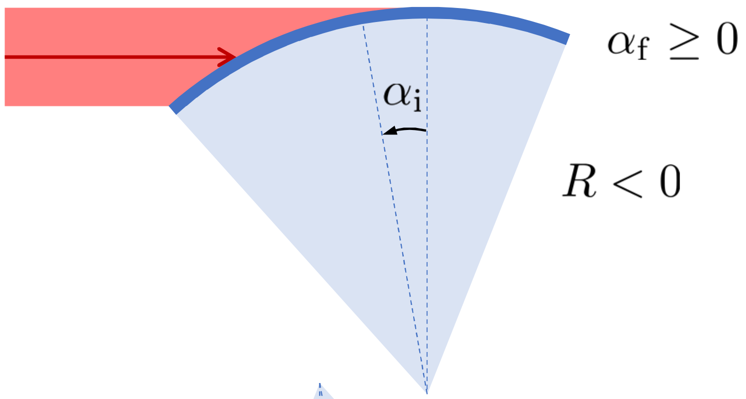

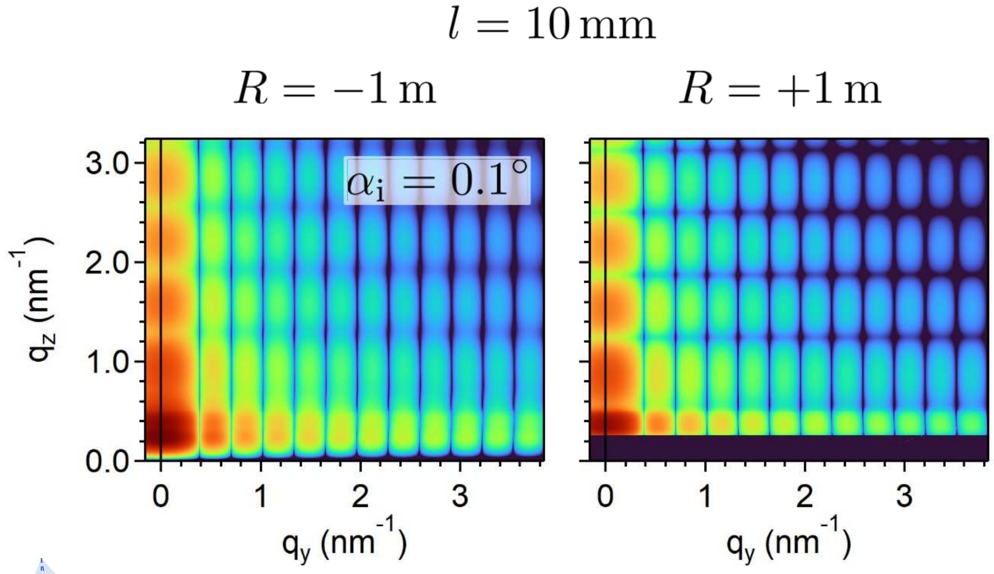

- Concave

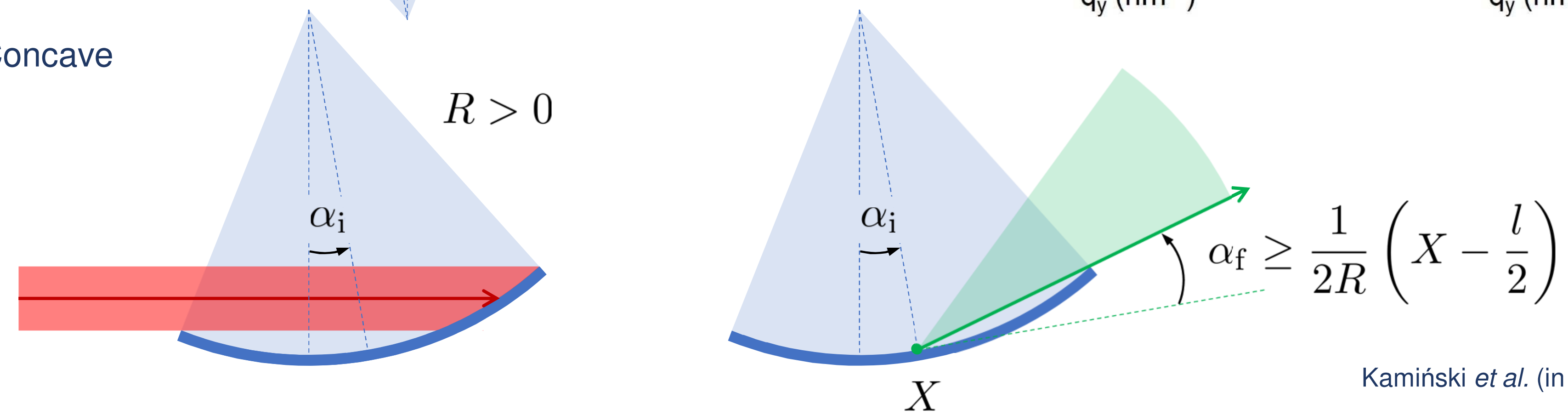

Kamiński *et al.* (in preparation)

GISAXS: some points of vigilance

Influence of the sample curvature

$$q_z = \frac{2\pi}{\lambda}\left[\sin(\alpha_f) + \sin(\alpha_i)\right]$$

- Convex

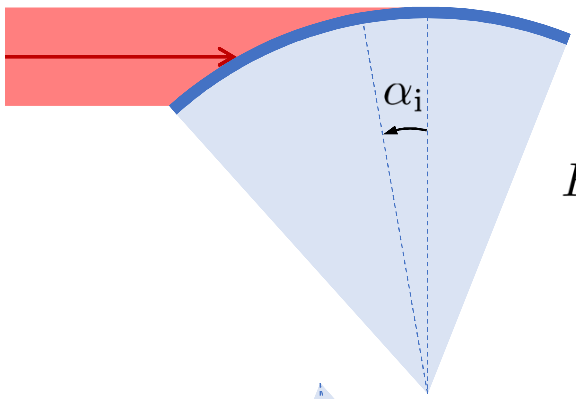

- Concave

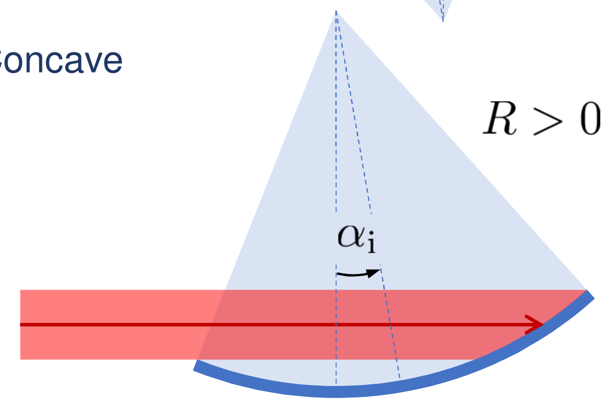

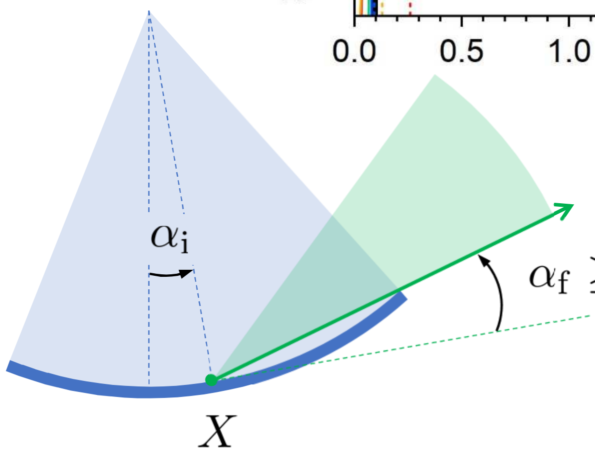

$$\alpha_f \geq \frac{1}{2R}\left(X - \frac{l}{2}\right)$$

$l = 10\,\mathrm{mm}$

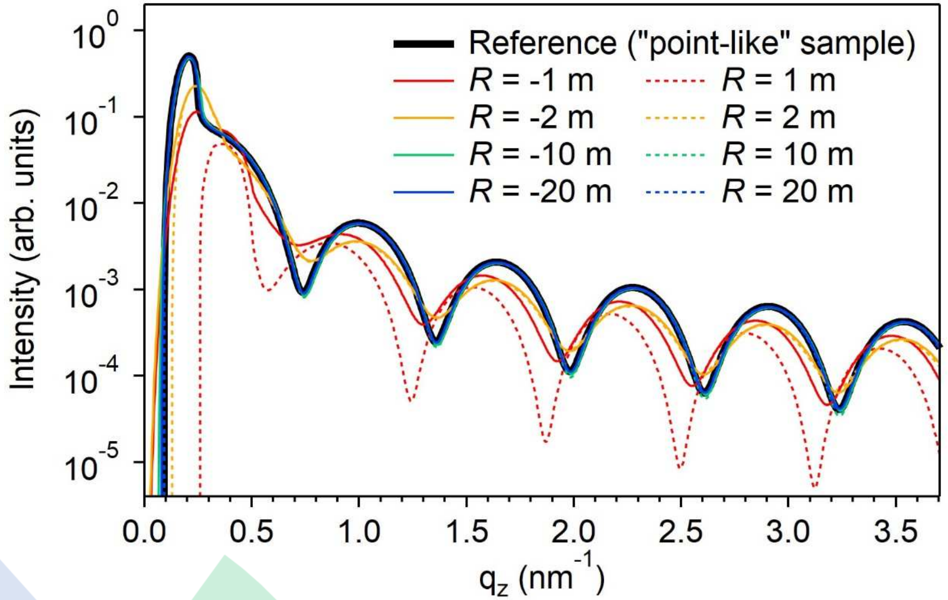

Kamiński *et al.* (in preparation)

Distorted Wave-Born Approximation (DWBA)

$$\alpha_\mathrm{i} \leq \alpha_\mathrm{c} \Rightarrow \left|\mathcal{R}\left(\alpha_\mathrm{i}\right)\right|^2 \approx 1$$

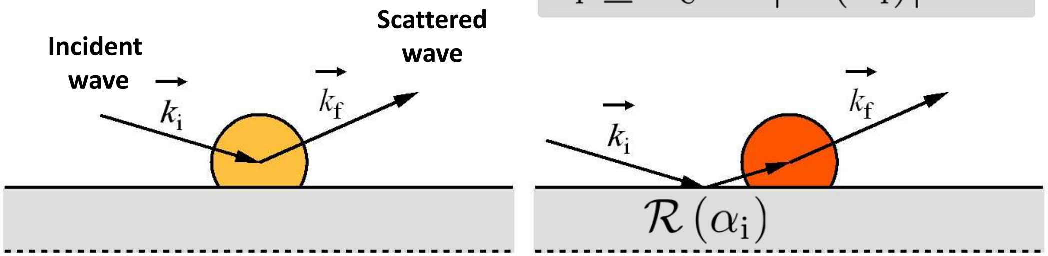

1 $q_\mathrm{z} = k_\mathrm{f,z} - k_\mathrm{i,z}$

2 $q_\mathrm{z} = k_\mathrm{f,z} + k_\mathrm{i,z}$

$$\mathcal{A}\left(\vec{q}\right) = F\left(q_\parallel, k_\mathrm{f,z} - k_\mathrm{i,z}\right) + \mathcal{R}\left(\alpha_\mathrm{i}\right) F\left(q_\parallel, k_\mathrm{f,z} + k_\mathrm{i,z}\right)$$

$$I\left(\vec{q}\right) = \left|\mathcal{A}\left(\vec{q}\right)\right|^2$$

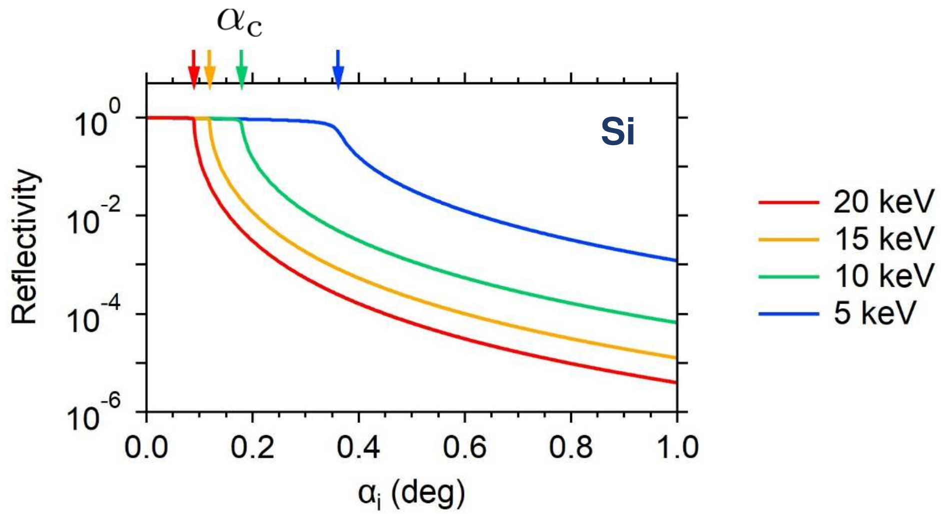

Distorted Wave-Born Approximation (DWBA)

$\alpha_{\mathrm{i}} \leq \alpha_{\mathrm{c}} \Rightarrow \left|\mathcal{R}\left(\alpha_{\mathrm{i}}\right)\right|^2 \approx 1$

$\alpha_{\mathrm{f}} \leq \alpha_{\mathrm{c}} \Rightarrow \left|\mathcal{R}\left(\alpha_{\mathrm{f}}\right)\right|^2 \approx 1$

1 $q_{\mathrm{z}} = k_{\mathrm{f,z}} - k_{\mathrm{i,z}}$

2 $q_{\mathrm{z}} = k_{\mathrm{f,z}} + k_{\mathrm{i,z}}$

3 $q_{\mathrm{z}} = -k_{\mathrm{f,z}} - k_{\mathrm{i,z}}$

4 $q_{\mathrm{z}} = -k_{\mathrm{f,z}} + k_{\mathrm{i,z}}$

$$\mathcal{A}\left(\vec{q}\right) = F\left(q_{\parallel}, k_{\mathrm{f,z}} - k_{\mathrm{i,z}}\right) + \mathcal{R}\left(\alpha_{\mathrm{i}}\right) F\left(q_{\parallel}, k_{\mathrm{f,z}} + k_{\mathrm{i,z}}\right) + \mathcal{R}\left(\alpha_{\mathrm{f}}\right) F\left(q_{\parallel}, -k_{\mathrm{f,z}} - k_{\mathrm{i,z}}\right) + \mathcal{R}\left(\alpha_{\mathrm{i}}\right)\mathcal{R}\left(\alpha_{\mathrm{f}}\right) F\left(q_{\parallel}, -k_{\mathrm{f,z}} + k_{\mathrm{i,z}}\right)$$

$$I\left(\vec{q}\right) = \left|\mathcal{A}\left(\vec{q}\right)\right|^2$$

Distorted Wave-Born Approximation (DWBA)

$\alpha_\mathrm{i} \leq \alpha_\mathrm{c} \Rightarrow |\mathcal{R}(\alpha_\mathrm{i})|^2 \approx 1$

$\alpha_\mathrm{f} \leq \alpha_\mathrm{c} \Rightarrow |\mathcal{R}(\alpha_\mathrm{f})|^2 \approx 1$

1. $q_\mathrm{z} = k_\mathrm{f,z} - k_\mathrm{i,z}$
2. $q_\mathrm{z} = k_\mathrm{f,z} + k_\mathrm{i,z}$
3. $q_\mathrm{z} = -k_\mathrm{f,z} - k_\mathrm{i,z}$
4. $q_\mathrm{z} = -k_\mathrm{f,z} + k_\mathrm{i,z}$

BA

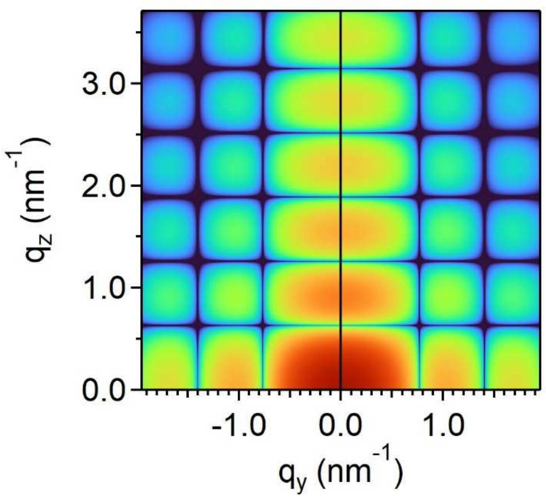

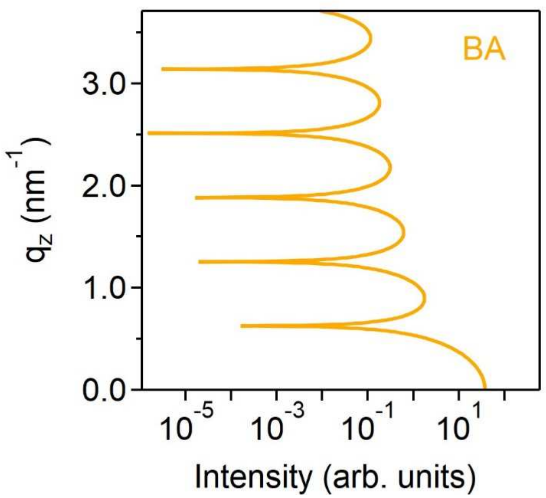

Ag cylinder

(D = 10 nm, H = 10 nm)

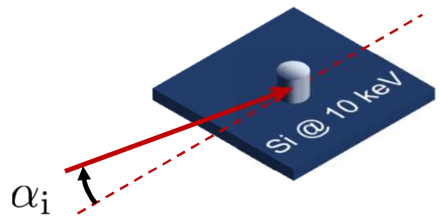

$(\alpha_\mathrm{c} = 0.179°)$

Distorted Wave-Born Approximation (DWBA)

$\alpha_\mathrm{i} \leq \alpha_\mathrm{c} \Rightarrow |\mathcal{R}(\alpha_\mathrm{i})|^2 \approx 1$

$\alpha_\mathrm{f} \leq \alpha_\mathrm{c} \Rightarrow |\mathcal{R}(\alpha_\mathrm{f})|^2 \approx 1$

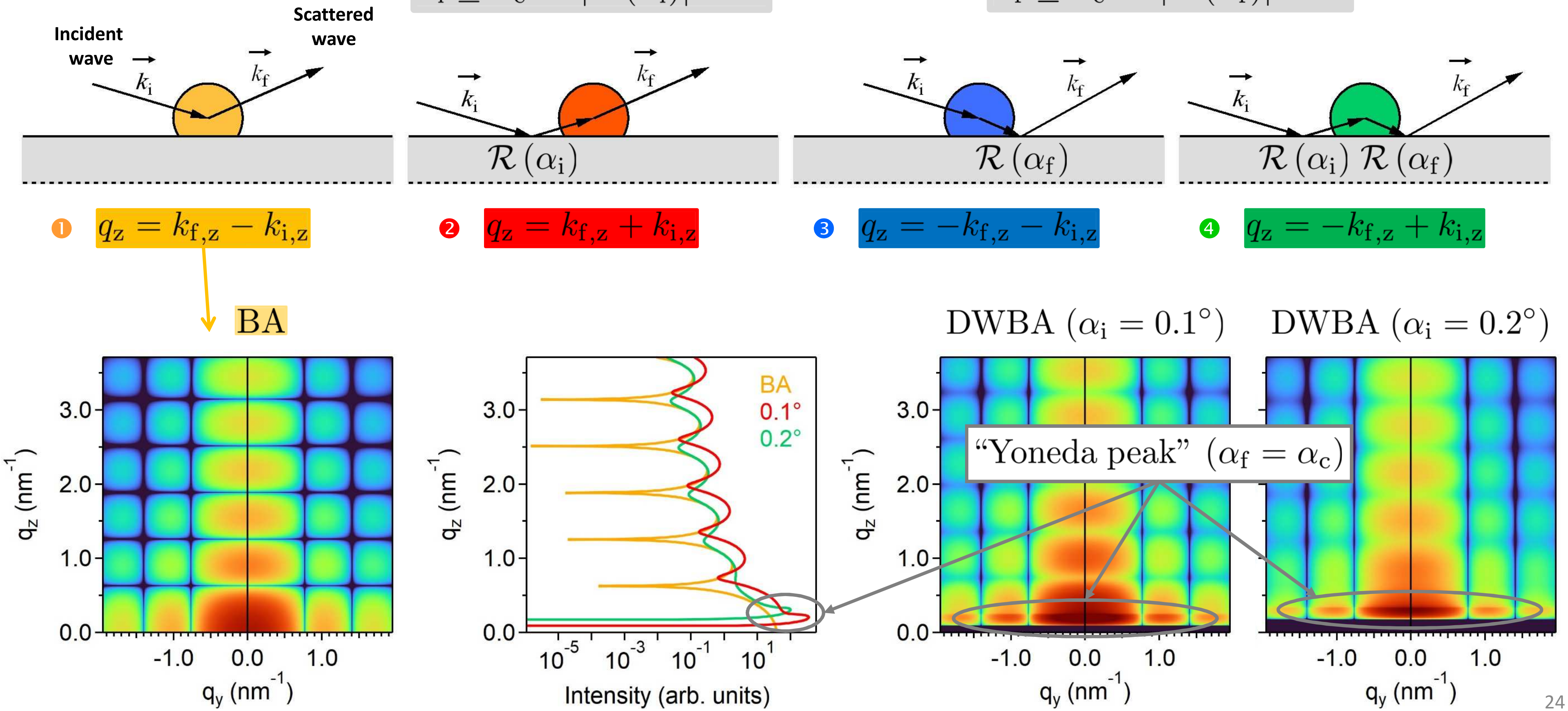

Distorted Wave-Born Approximation (DWBA)

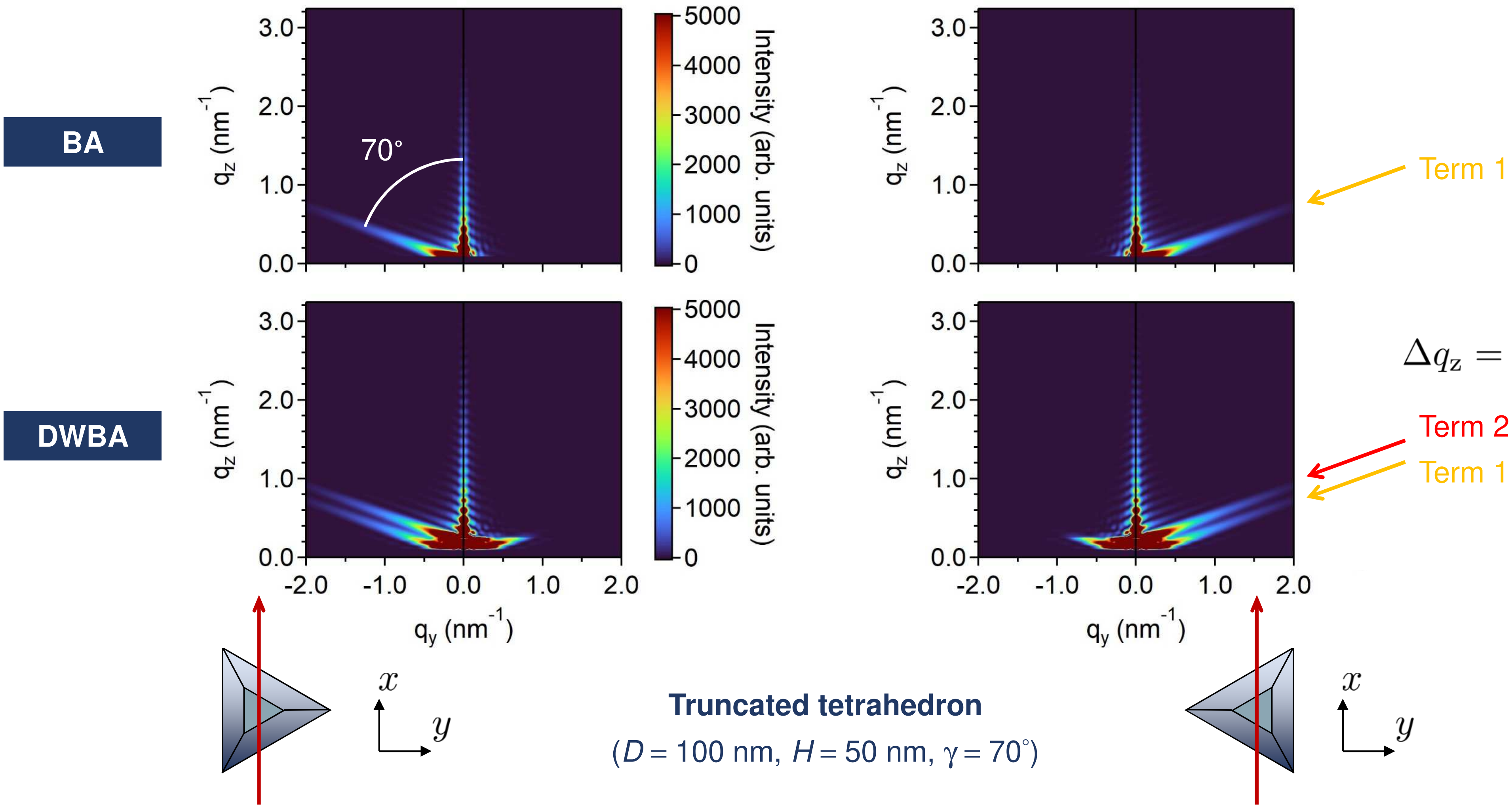

$$\Delta q_z = \frac{4\pi}{\lambda}\sin\alpha_i$$

Truncated tetrahedron

($D = 100$ nm, $H = 50$ nm, $\gamma = 70°$)

Distorted Wave-Born Approximation (DWBA)

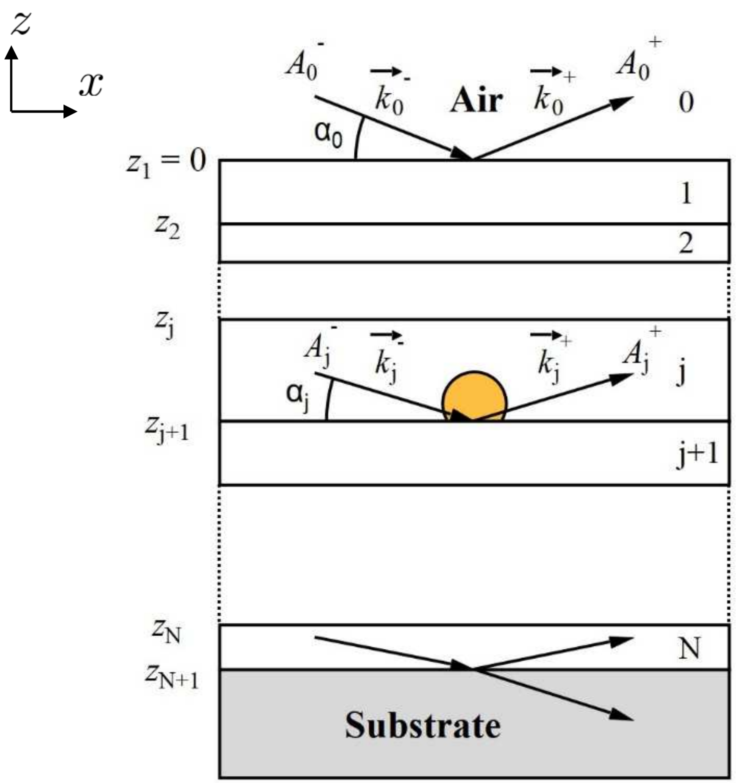

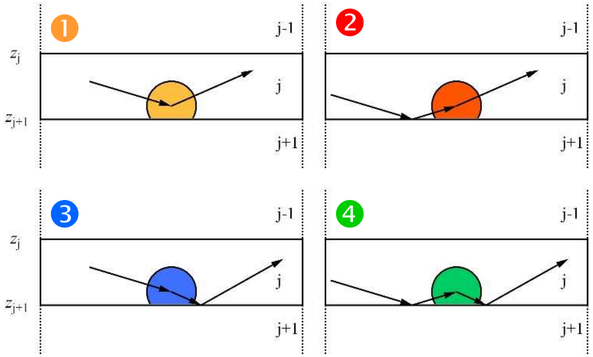

$$k_{z,j}^{\pm} = \pm \frac{2\pi}{\lambda} \sqrt{n_j^2 - \cos^2 \alpha_0}$$

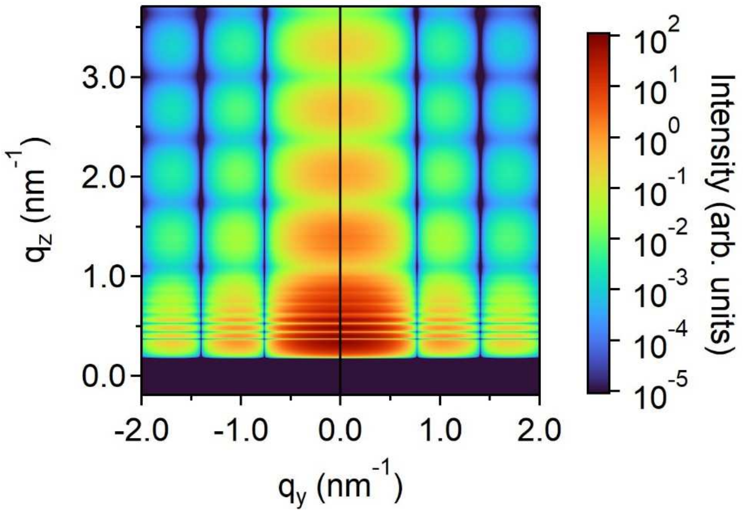

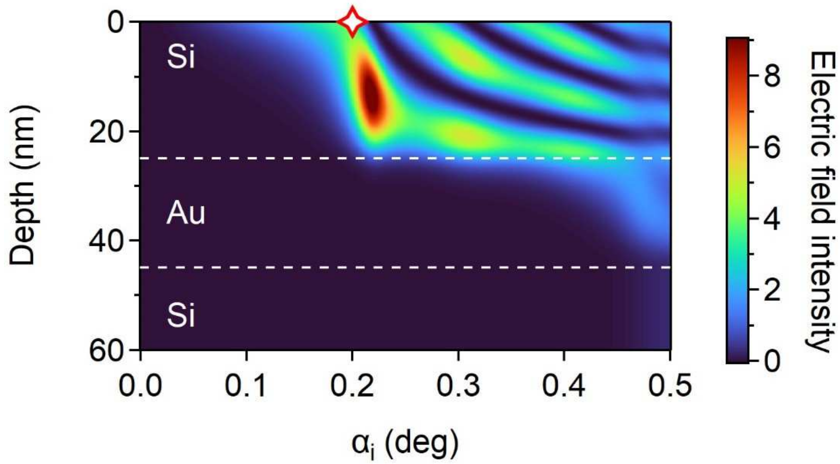

Ag cylinder @ 10 keV

$$D = H = 10\,\mathrm{nm}$$

$$\alpha_i = 0.2^\circ$$

$$z = 0$$

Distorted Wave-Born Approximation (DWBA)

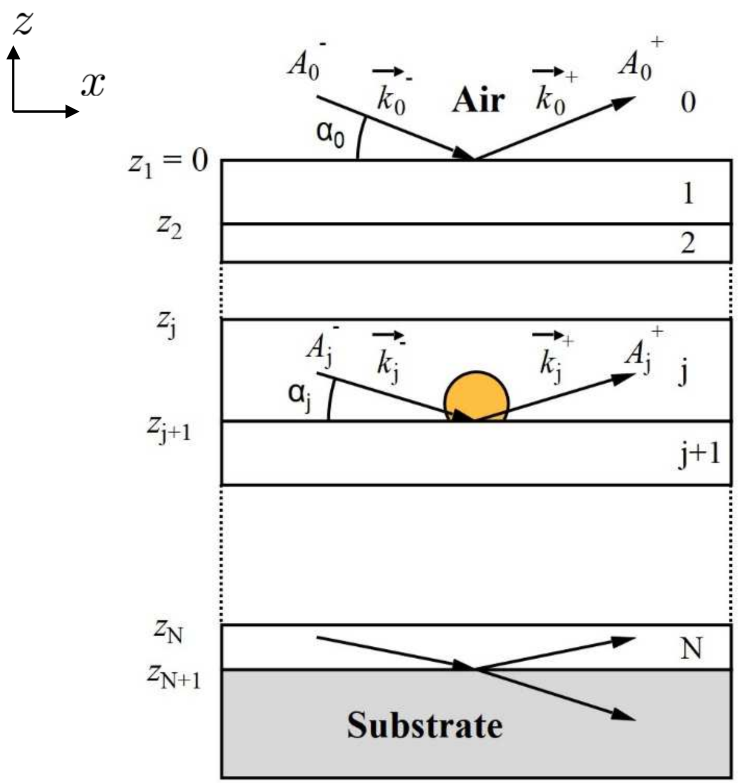

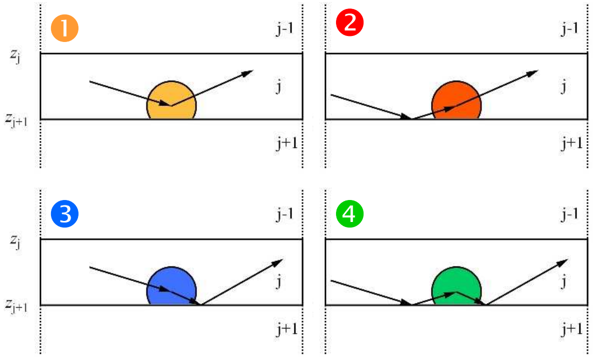

$$k^{\pm}_{z,j} = \pm\frac{2\pi}{\lambda}\sqrt{n_j^2 - \cos^2\alpha_0}$$

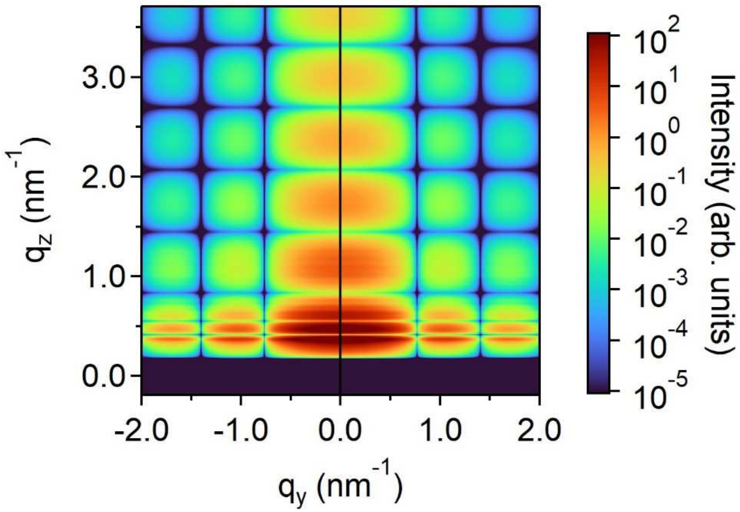

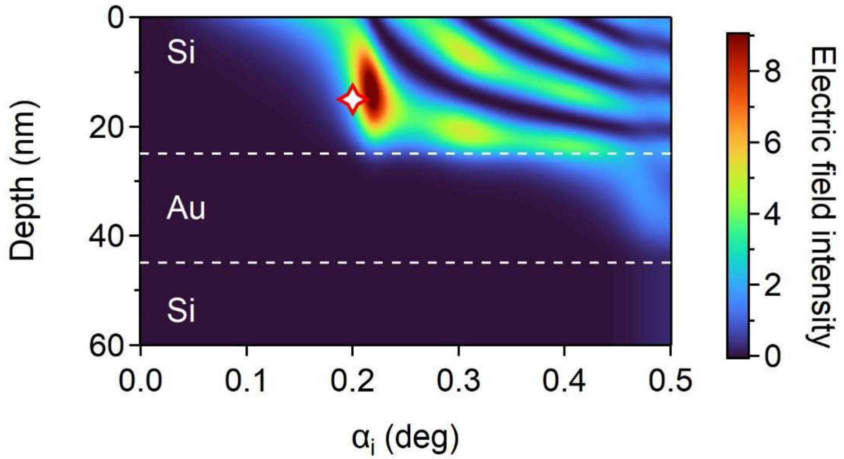

Ag cylinder @ 10 keV

$$D = H = 10\,\text{nm}$$

$$\alpha_\text{i} = 0.2^\circ$$

$$z = 15\,\text{nm}$$

Distorted Wave-Born Approximation (DWBA)

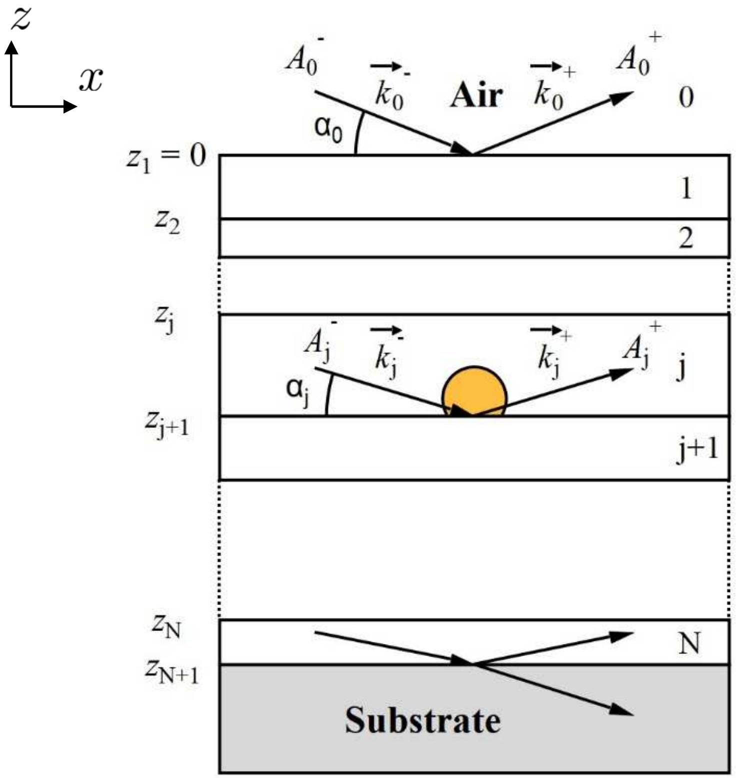

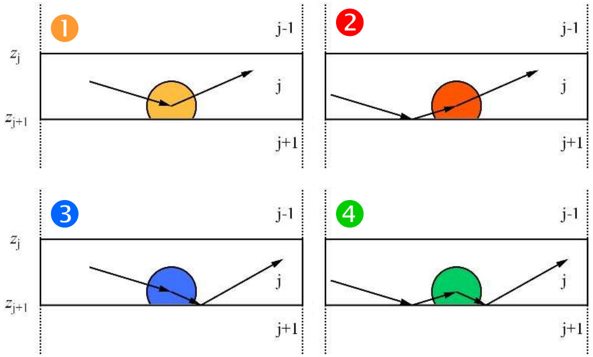

$$k^{\pm}_{z,j} = \pm\frac{2\pi}{\lambda}\sqrt{n_j^2 - \cos^2\alpha_0}$$

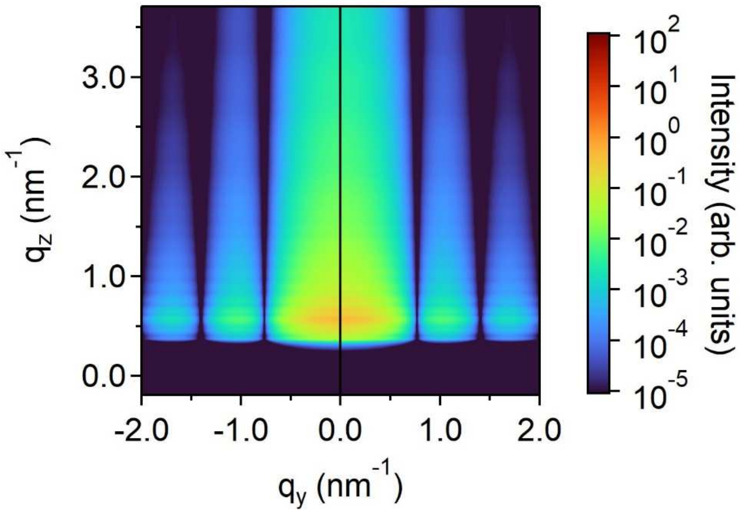

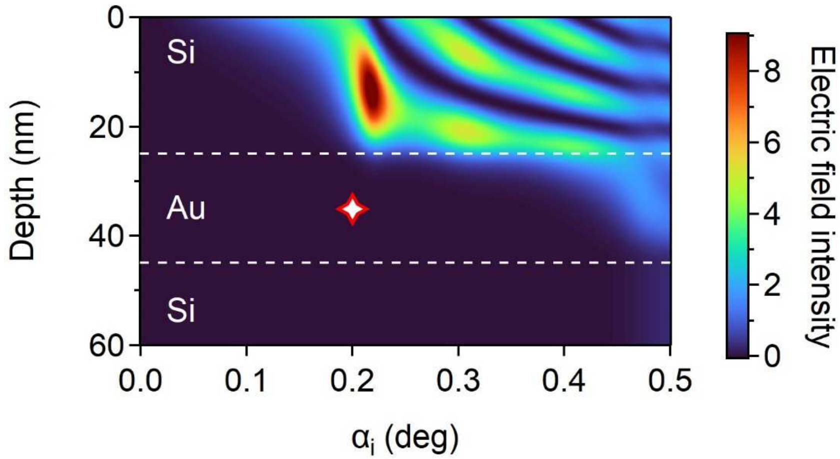

Ag cylinder @ 10 keV

$$D = H = 10\,\mathrm{nm}$$

$$\alpha_\mathrm{i} = 0.2^\circ$$

$$z = 35\,\mathrm{nm}$$

Distorted Wave-Born Approximation (DWBA)

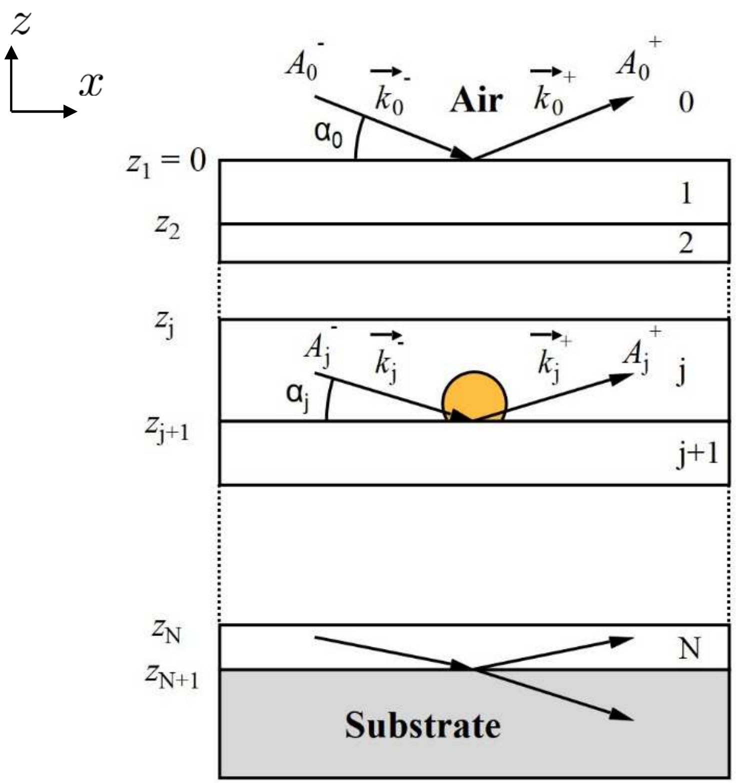

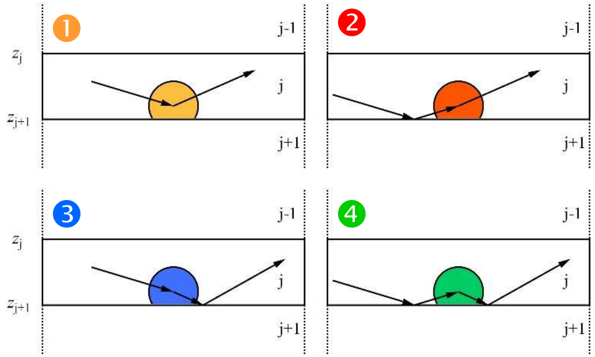

$$k_{z,j}^{\pm} = \pm \frac{2\pi}{\lambda} \sqrt{n_j^2 - \cos^2 \alpha_0}$$

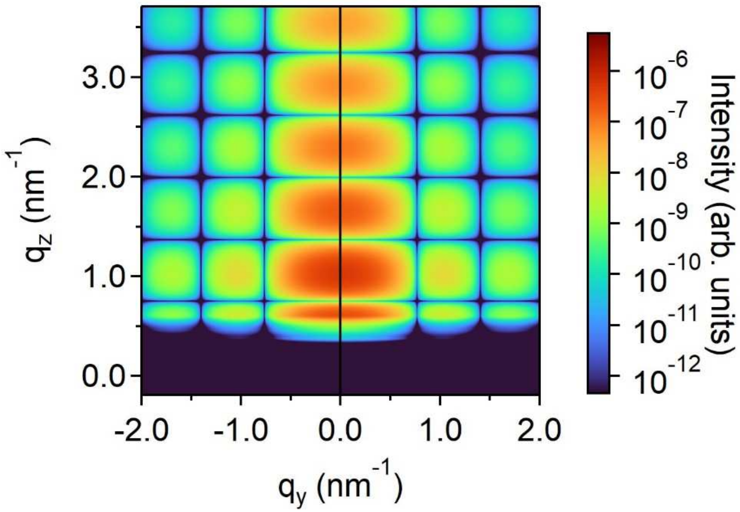

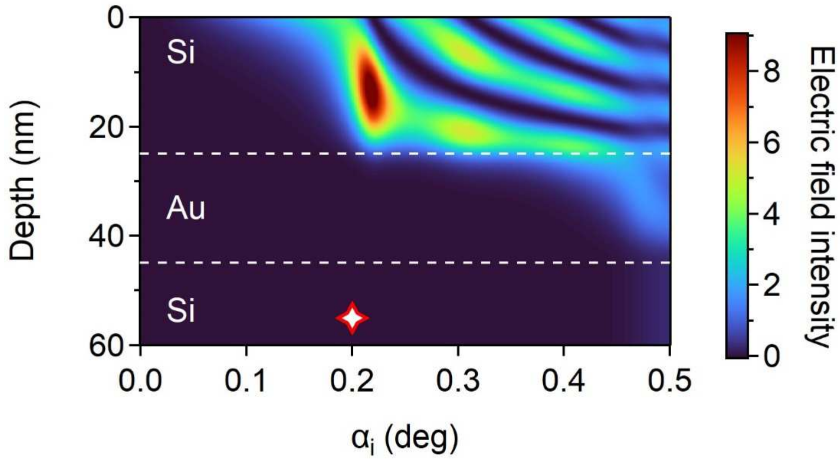

Ag cylinder @ 10 keV

$$D = H = 10\,\text{nm}$$

$$\alpha_\text{i} = 0.2^\circ$$

$$z = 55\,\text{nm}$$

Gold islands sandwiched between carbon layers

System Si / Ni / C / Au / C

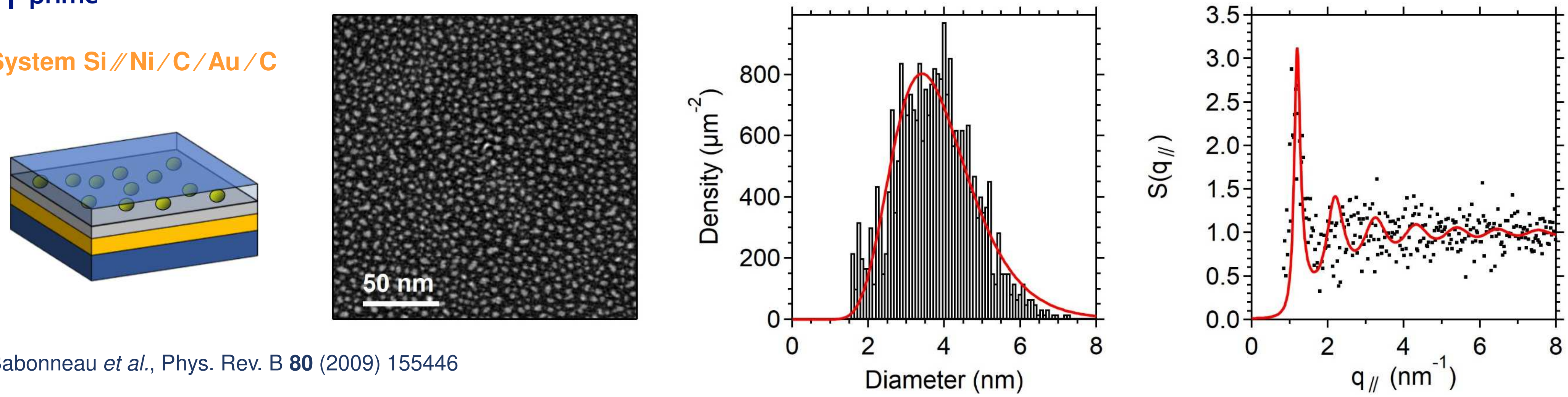

Babonneau *et al.*, Phys. Rev. B **80** (2009) 155446

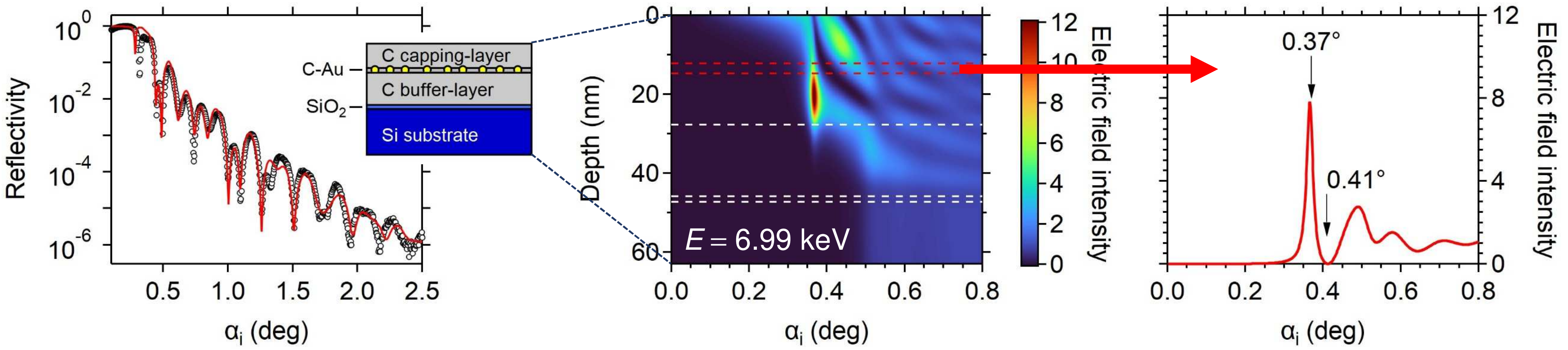

Gold islands sandwiched between carbon layers

System Si ⁄ Ni ⁄ C ⁄ Au ⁄ C

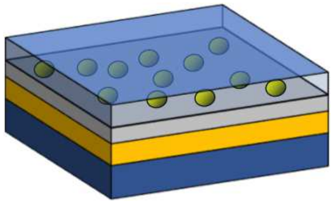

Babonneau *et al.*, Phys. Rev. B **80** (2009) 155446

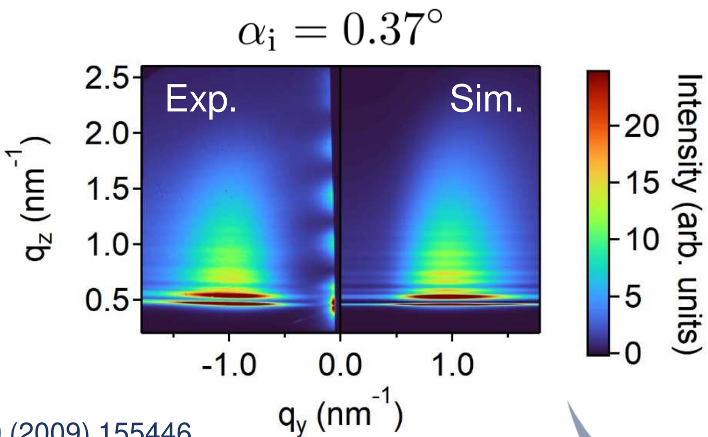

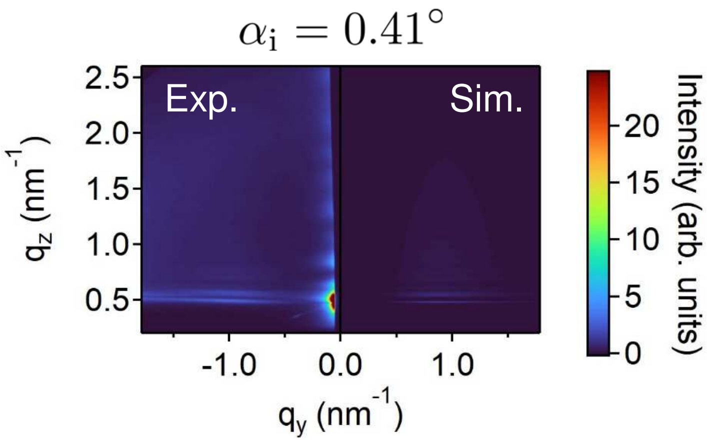

$E = 6.99$ keV

$$I\left(q_{\parallel}, q_z\right) \propto \int_0^{\infty} \underbrace{\left|\mathcal{A}\left(q_{\parallel}, q_z\right)\right|^2} \underbrace{S\left(q_{\parallel}\right)} \underbrace{N\left(D\right)} dD$$

$$H = f(D)$$

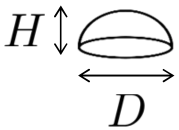

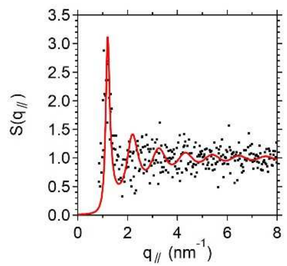

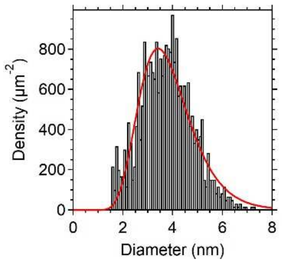

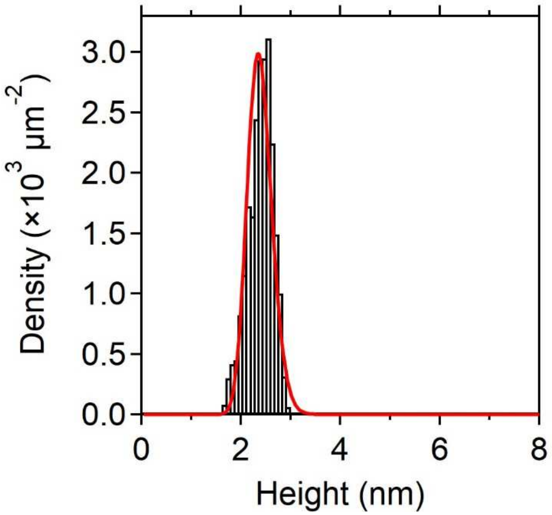

Photochromic Ag/TiO_2 thin films

nature materials | VOL 2 | JANUARY 2003 | www.nature.com/naturematerials

LETTERS

Multicolour photochromism of TiO_2 films loaded with silver nanoparticles

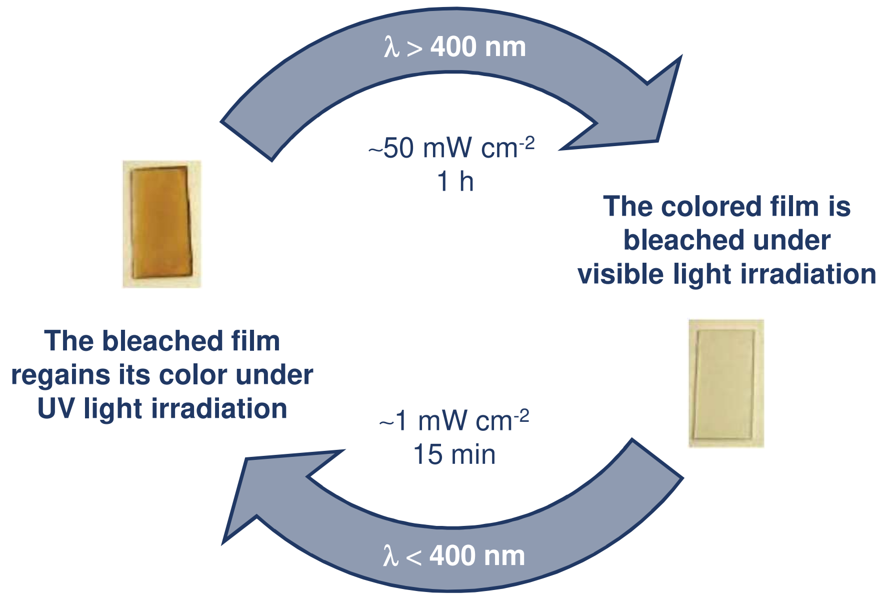

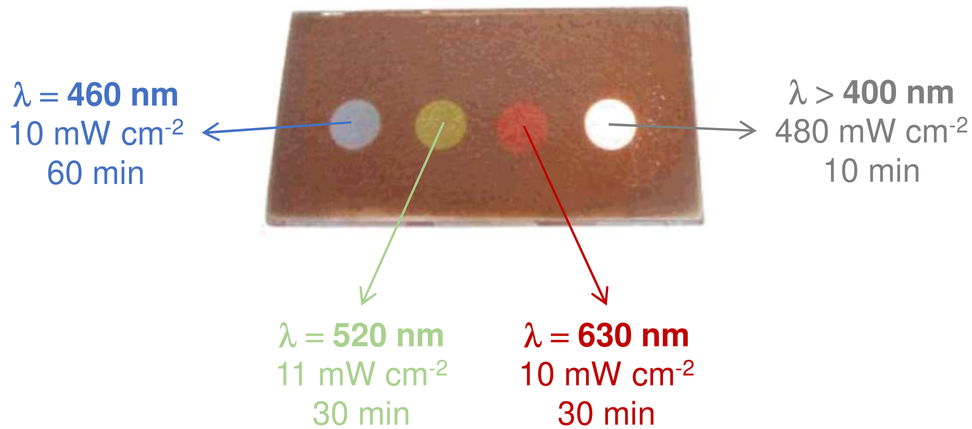

- **Vis. light**: Size-selective Ag oxidation by photo-induced electron transfer at the localized surface plasmon resonance
- **UV light**: Photocatalytic reduction of the Ag^+ ions to metallic Ag

Ohko *et al.*, Nat. Mater. **2** (2003) 29
Naoi *et al.*, J. Am. Chem. Soc. **126** (2004) 3664

Photochromic Ag/TiO_2 thin films

ADVANCED MATERIALS
www.advmat.de

Materials Views
www.MaterialsViews.com

Reversible and Irreversible Laser Microinscription on Silver-Containing Mesoporous Titania Films

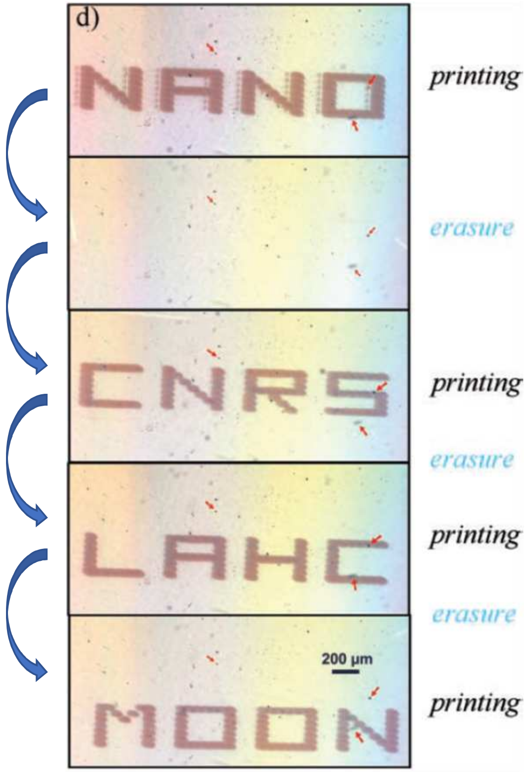

λ_{UV} = 244 nm
30 kW cm^{-2}
150 ms

λ_{vis} = 488 nm
75 W cm^{-2}
10 min

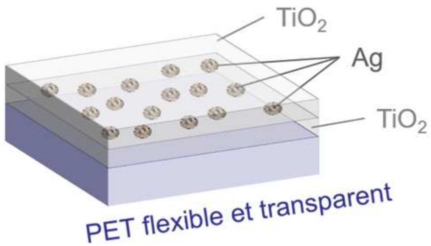

λ_{vis} = 647 nm

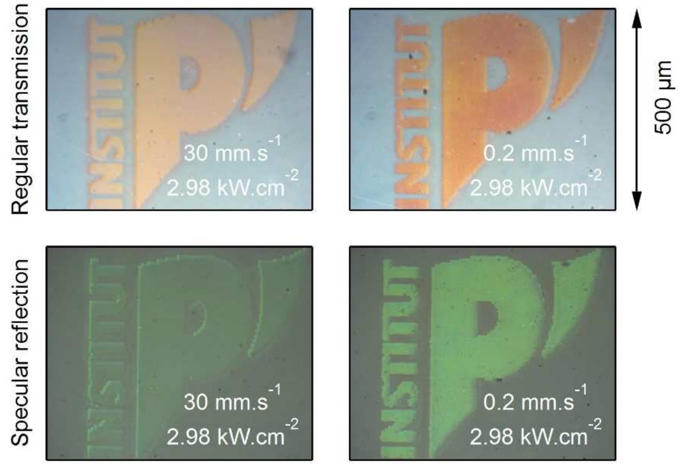

Crespo-Monteiro *et al.*, Adv. Mater. **22** (2010) 3166
Diop *et al.*, Appl. Spectrosc. **6** (2017) 1271

Photochromic Ag/TiO_2 thin films

Real-time investigations under UV and visible laser irradiation

Coll. N. Destouches

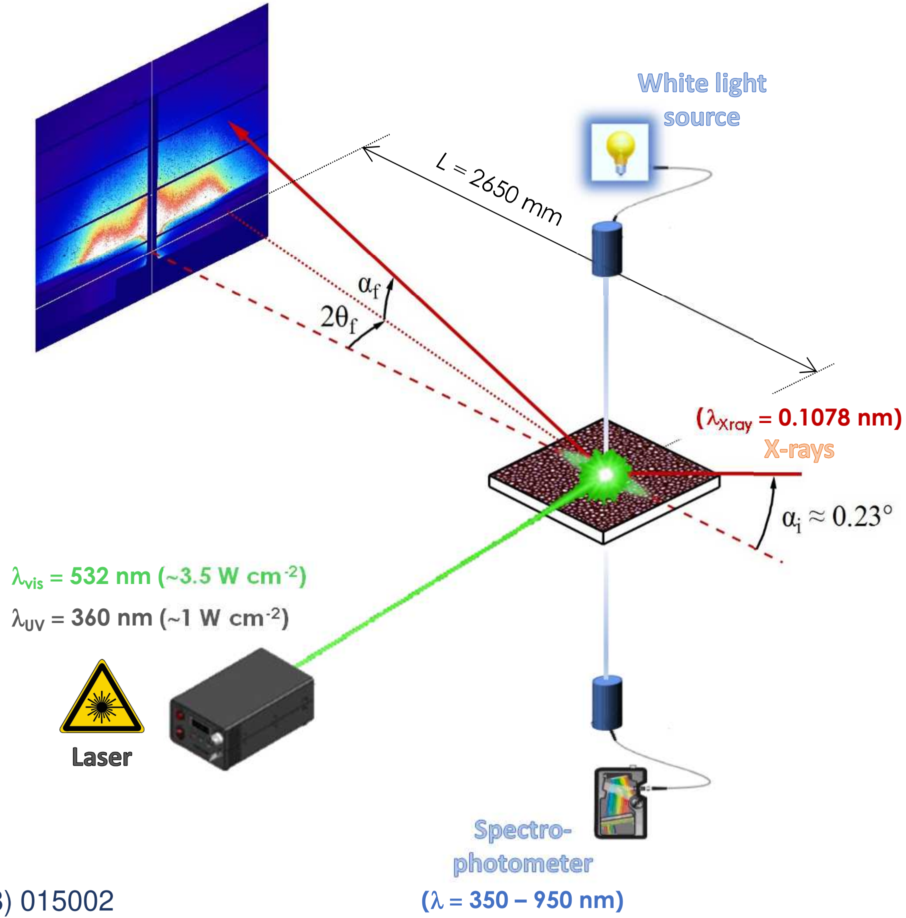

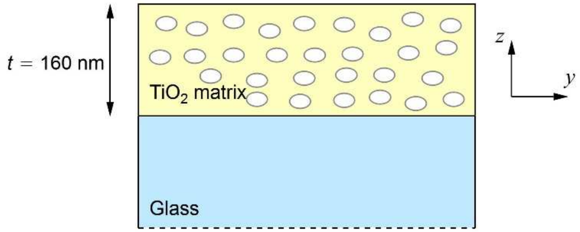

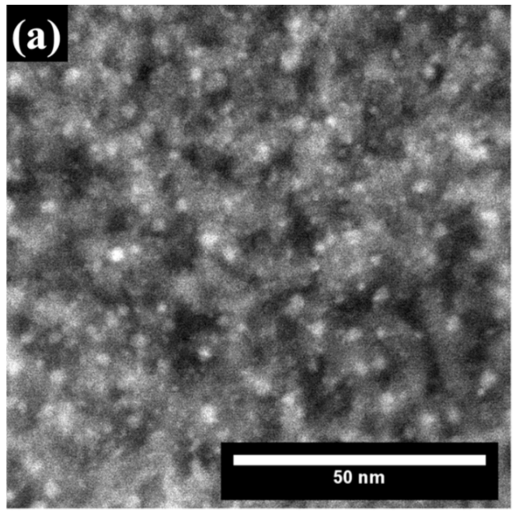

E = 11.5 keV

Ag nanoparticles grown in a nanoporous TiO_2 film by reduction after immersion into an aqueous ammoniacal silver solution

- Film thickness: ~160 nm
- Pore diameter: ~8 nm

Babonneau *et al.*, Nano Futures **2** (2018) 015002

Photochromic Ag/TiO_2 thin films

Real-time investigations under UV and visible laser irradiation

Coll. N. Destouches

Laboratoire Hubert Curien
UMR • CNRS • 5516 • Saint-Étienne

ESRF
The European Synchrotron

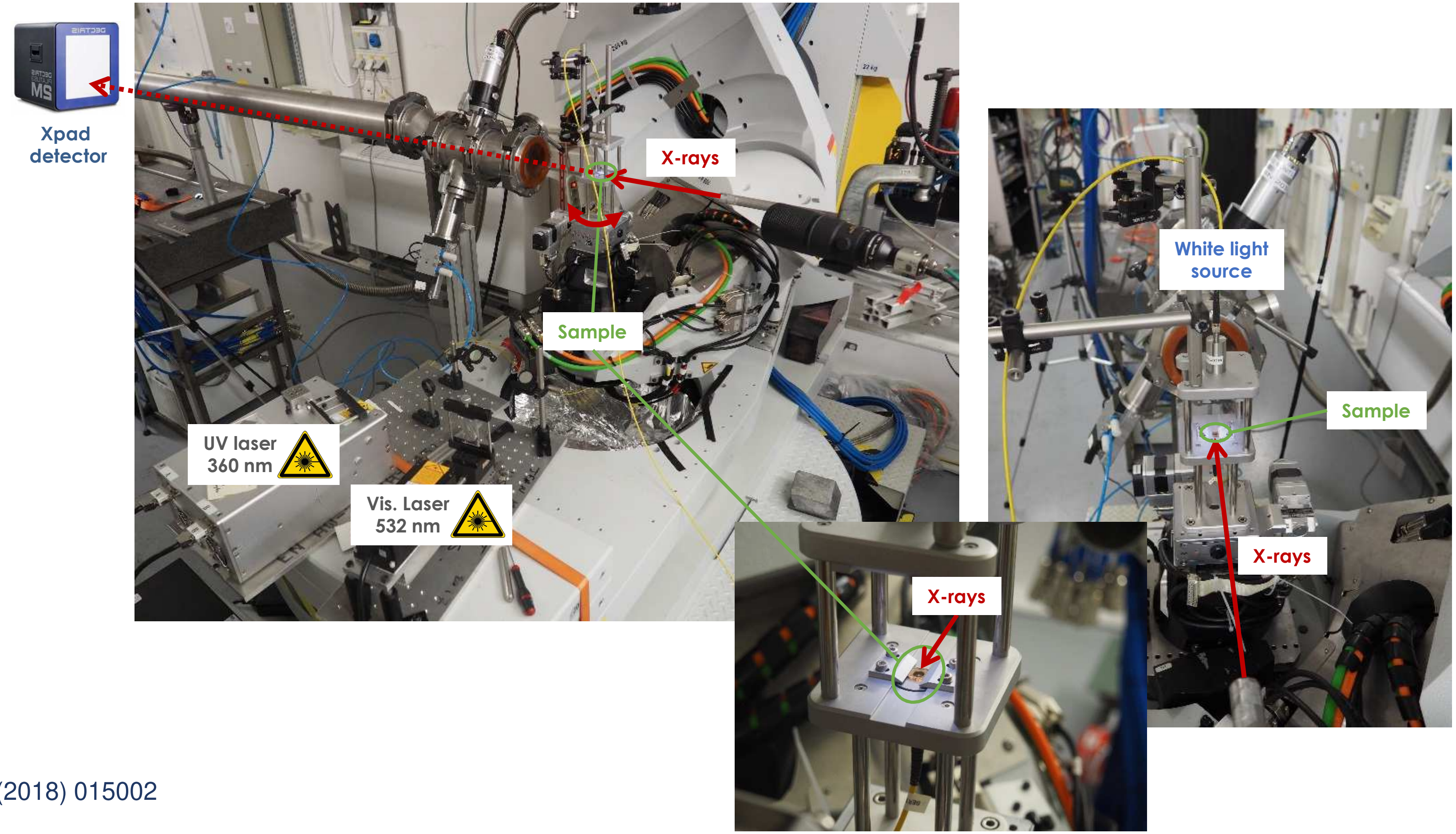

$E = 11.5$ keV

Babonneau *et al.*, Nano Futures **2** (2018) 015002

Photochromic Ag/TiO_2 thin films

Real-time investigations under UV and visible laser irradiation

Coll. N. Destouches

Laboratoire Hubert Curien UMR • CNRS • 5516 • Saint-Étienne

ESRF The European Synchrotron

$E = 11.5$ keV

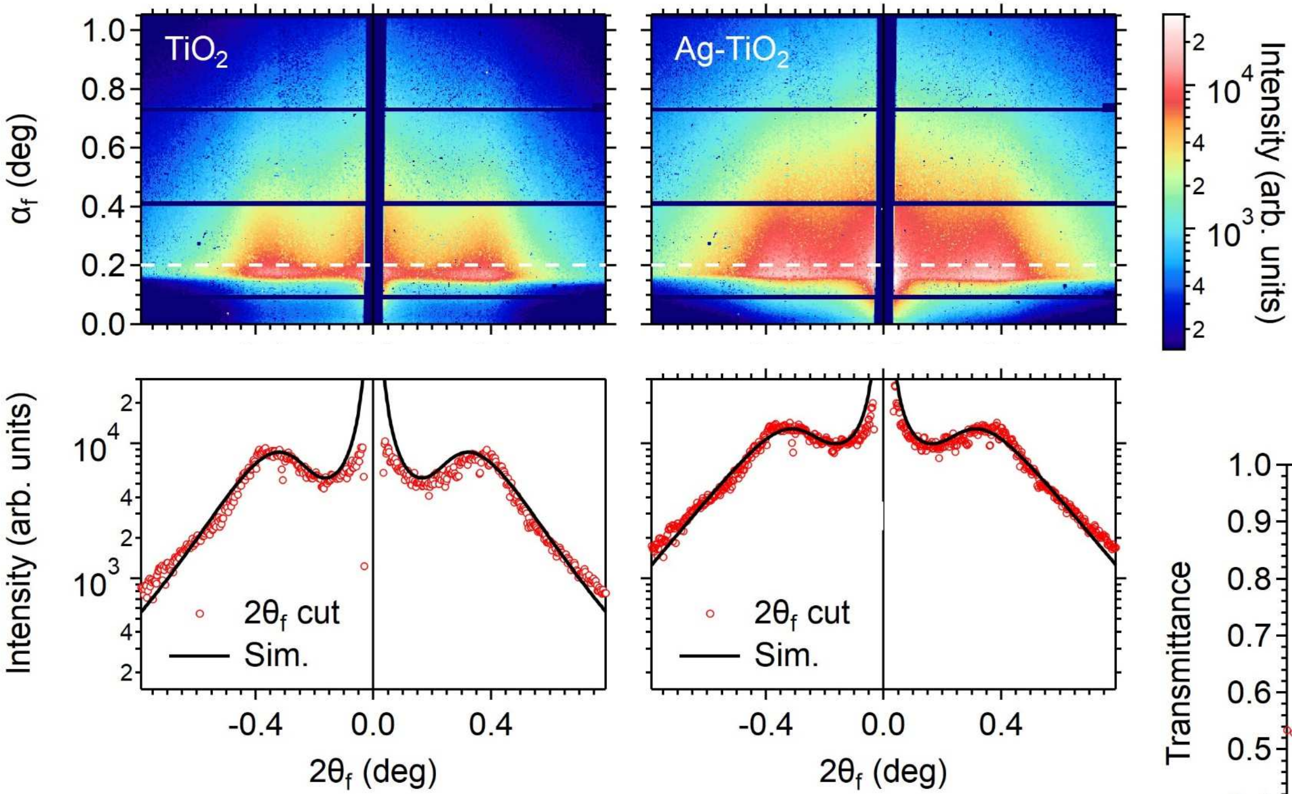

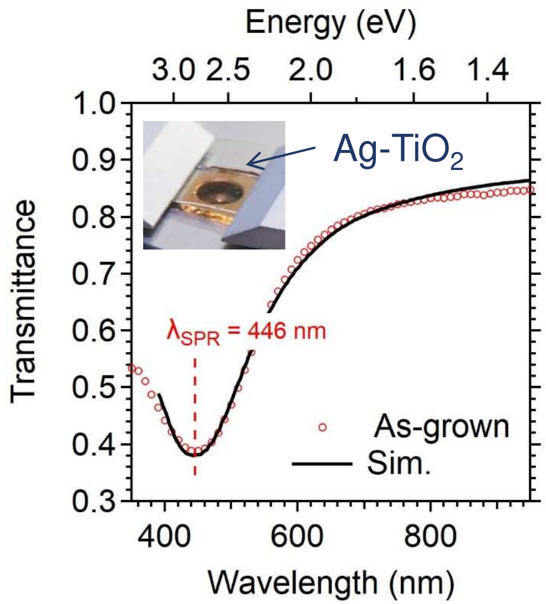

TiO_2	Pores	$D = 7.8$ nm	$H/D = 0.72$
Ag-TiO_2	Ag NPs	$D = 6.8$ nm	$H/D = 0.77$

Babonneau *et al.*, Nano Futures **2** (2018) 015002

Photochromic Ag/TiO_2 thin films

Real-time investigations under UV and visible laser irradiation

Coll. N. Destouches

Laboratoire Hubert Curien
UMR • CNRS • 5516 • Saint-Étienne

ESRF
The European Synchrotron

$E = 11.5$ keV

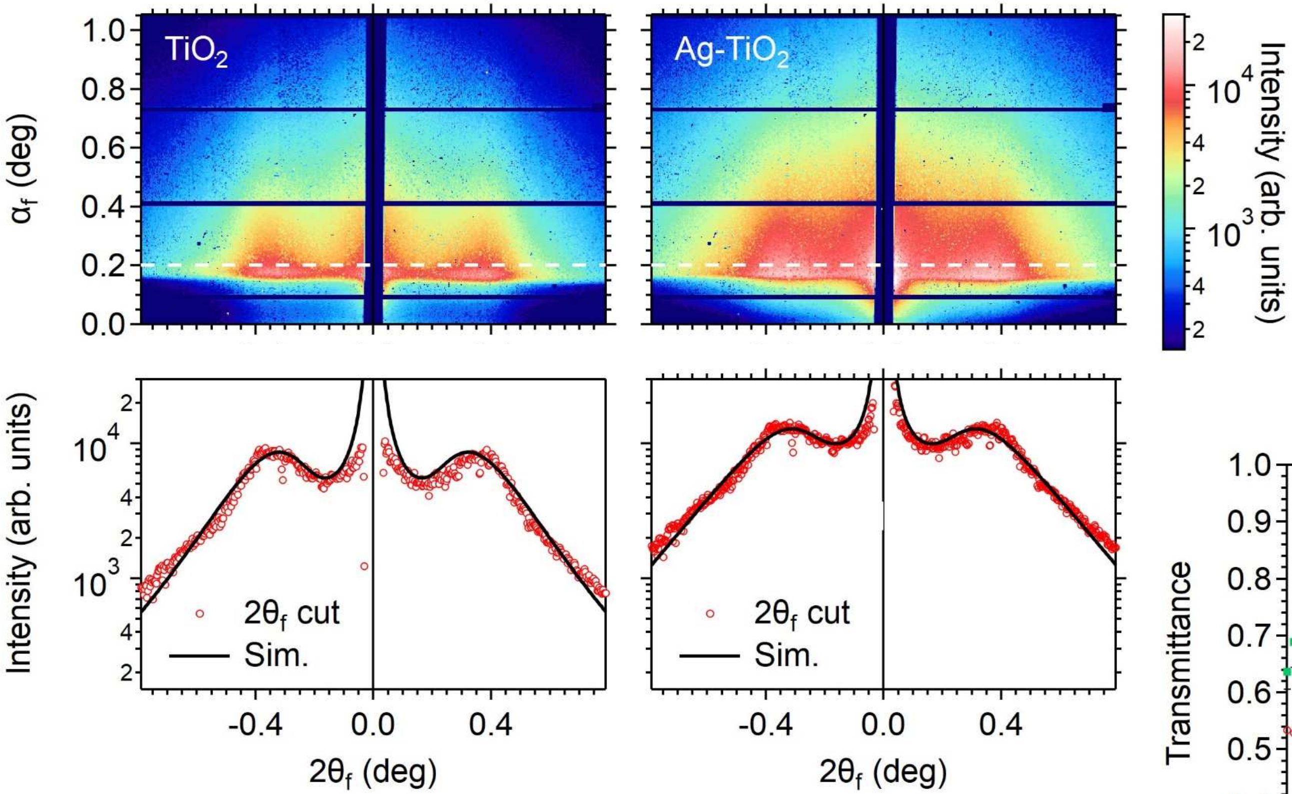

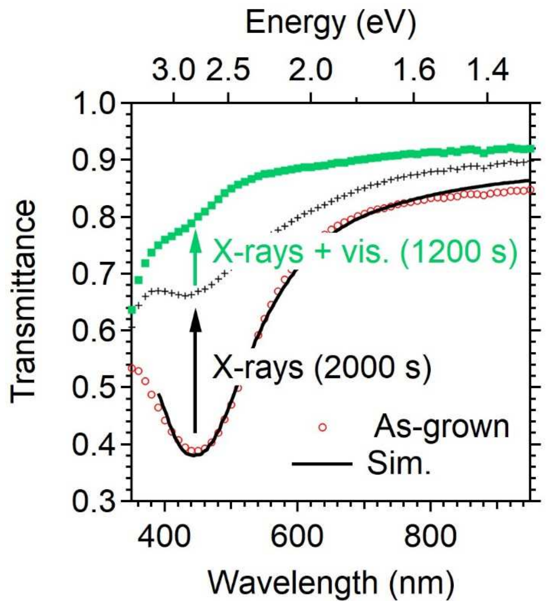

TiO_2	Pores	$D = 7.8$ nm	$H/D = 0.72$
Ag-TiO_2	Ag NPs	$D = 6.8$ nm	$H/D = 0.77$

Babonneau *et al.*, Nano Futures **2** (2018) 015002

Photochromic Ag/TiO_2 thin films

Real-time investigations under UV and visible laser irradiation

Coll. N. Destouches

Laboratoire Hubert Curien
UMR • CNRS • 5516 • Saint-Étienne

ESRF
The European Synchrotron

d²am

$E = 11.5$ keV

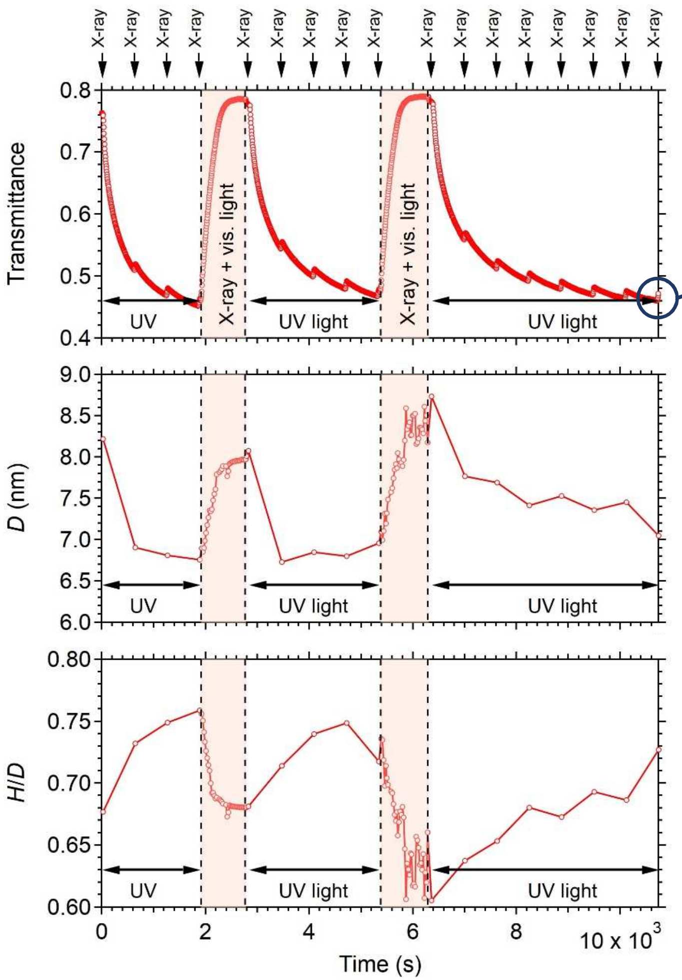

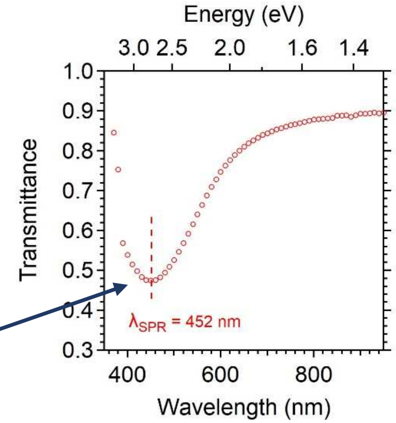

- Repeatable photochromic behavior with a good contrast between the colored and colorless states
- Photo-oxidation process (X-ray + vis.) is always faster than the photocatalytic reduction process (UV)
- Efficiency of the photo-activated reduction process (UV exposure) is degraded after 2 cycles

Babonneau *et al.*, Nano Futures **2** (2018) 015002

In situ and real-time studies of ultrathin silver films

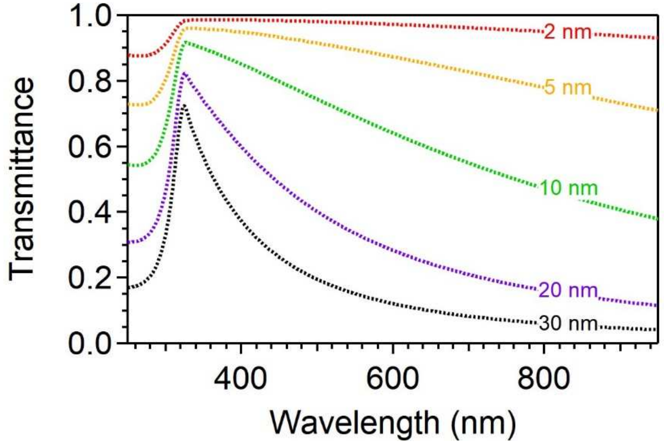

Simulation
'Ideal case'

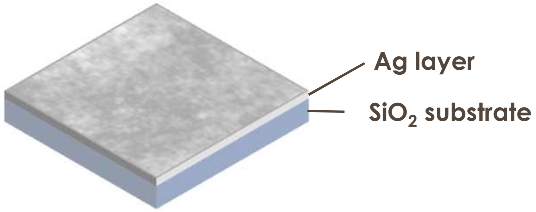

- **Ultrathin Ag layers (thickness t_{Ag} < 10 nm)**
  - High optical transmittance (vis.) / reflectance (IR)
  - High electrical conductivity
  - High thermal conductivity
  - High ductility

Flexible electronics

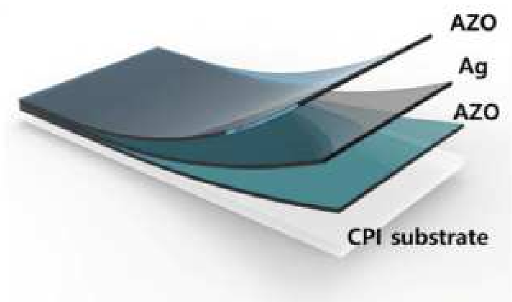

Kim *et al.*, Mater. Res. Bull. **149** (2022) 111703

Low-emissivity glazing

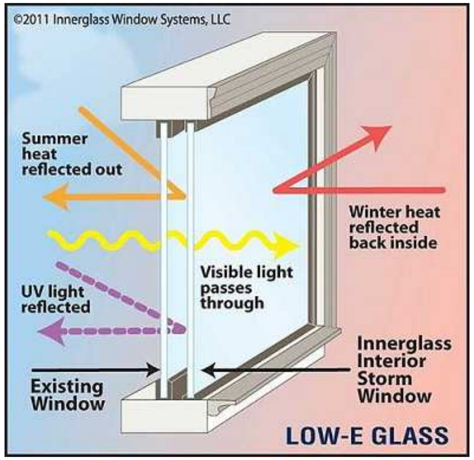

https://energyeducation.ca/encyclopedia/E-coating

In situ and real-time studies of ultrathin silver films

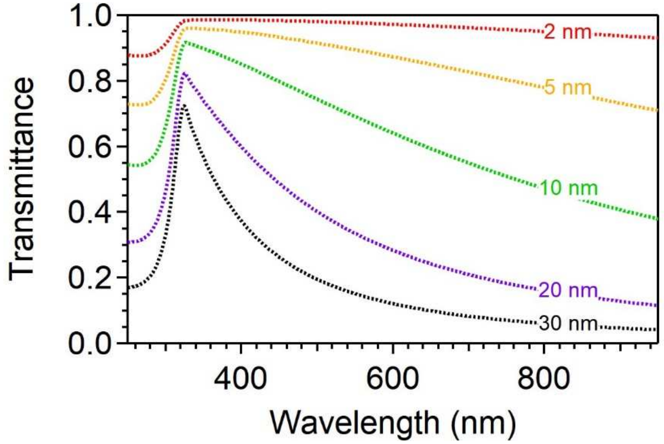

Simulation
'Ideal case'

≠

Experiment
'Real case'

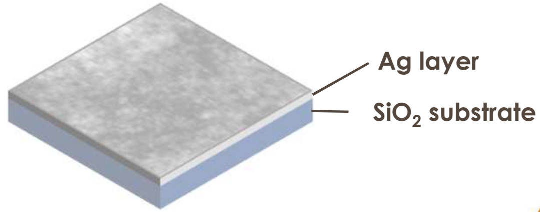

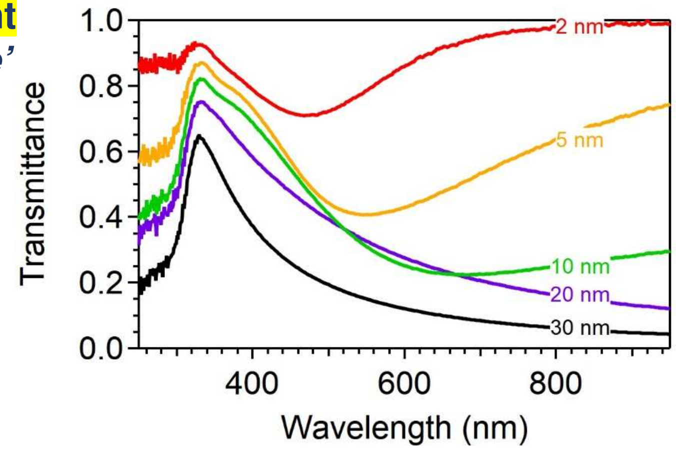

t_{Ag} = 1.3 nm t_{Ag} = 2.5 nm t_{Ag} = 6.3 nm t_{Ag} = 10.1 nm

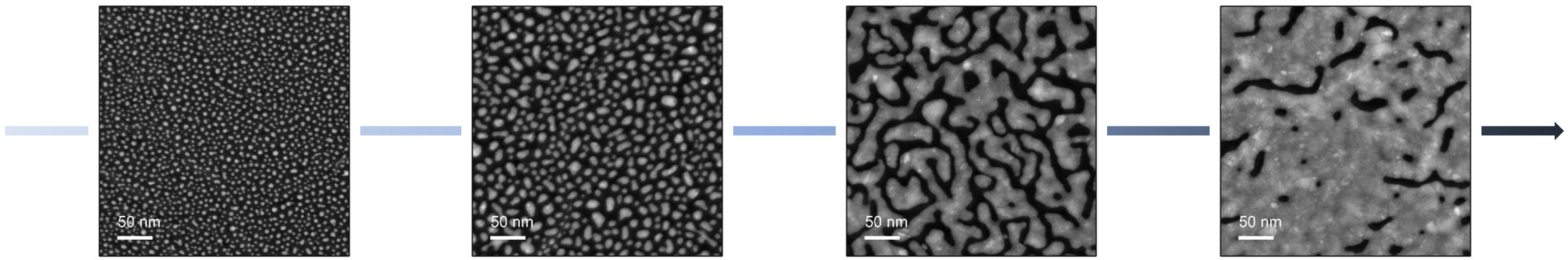

Simonot *et al.*, Appl. Surf. Sci. **544** (2021) 148672

Room temperature magnetron sputtering deposition Si_3N_4 / Ag (t_{Ag}) / Si_3N_4

- **Early stages dominated by strong optical absorption (localized surface plasmon resonance) and high electrical resistivity**
- **Growth strategies needed for producing conductive and transparent Ag layers ➨ use of gas additives (*e.g.*, O_2, N_2, etc.)**

In situ and real-time studies of ultrathin silver films

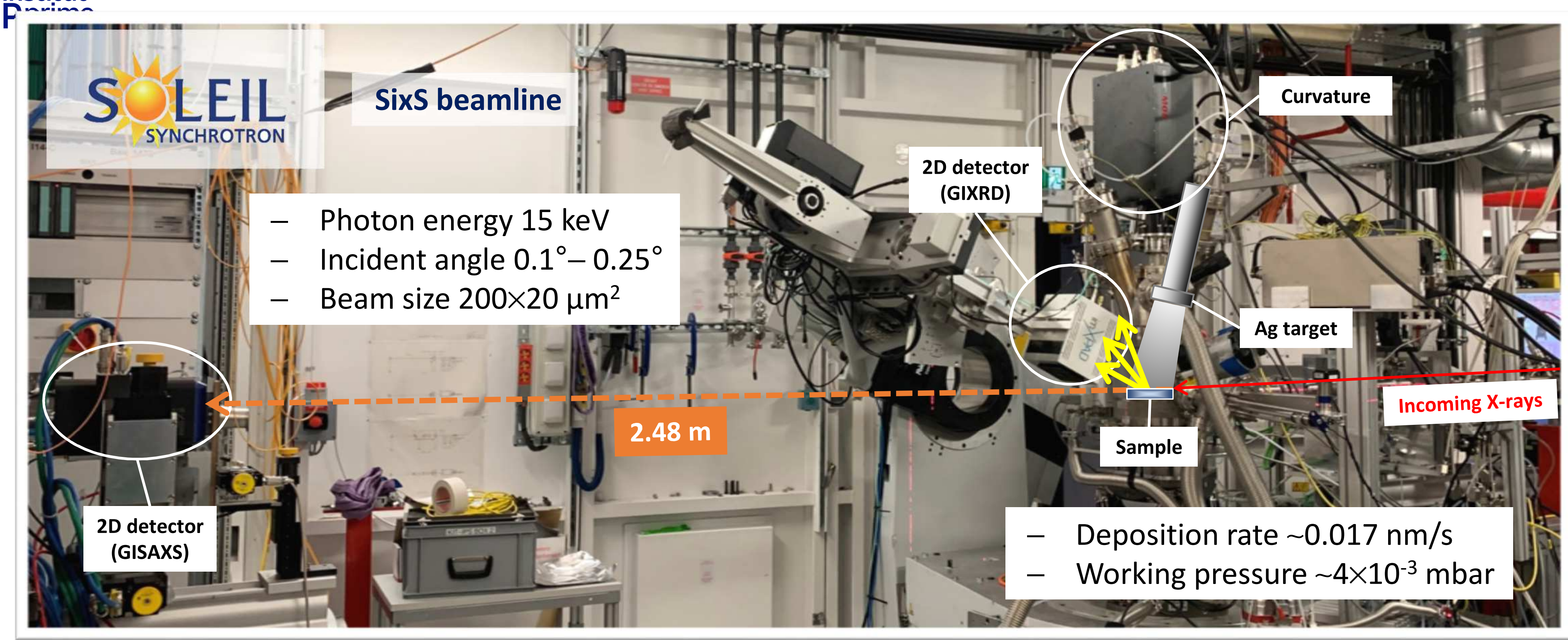

- **Simultaneous measurements during magnetron sputtering Ag deposition on SiO_x/Si**
  - GISAXS: island morphology and organization
  - GID: crystal structure, grain size and orientation…
  - Substrate curvature measurements: stress evolution

KIT Karlsruher Institut für Technologie

anr agence nationale de la recherche AU SERVICE DE LA SCIENCE

DFG Deutsche Forschungsgemeinschaft

In situ and real-time studies of ultrathin silver films

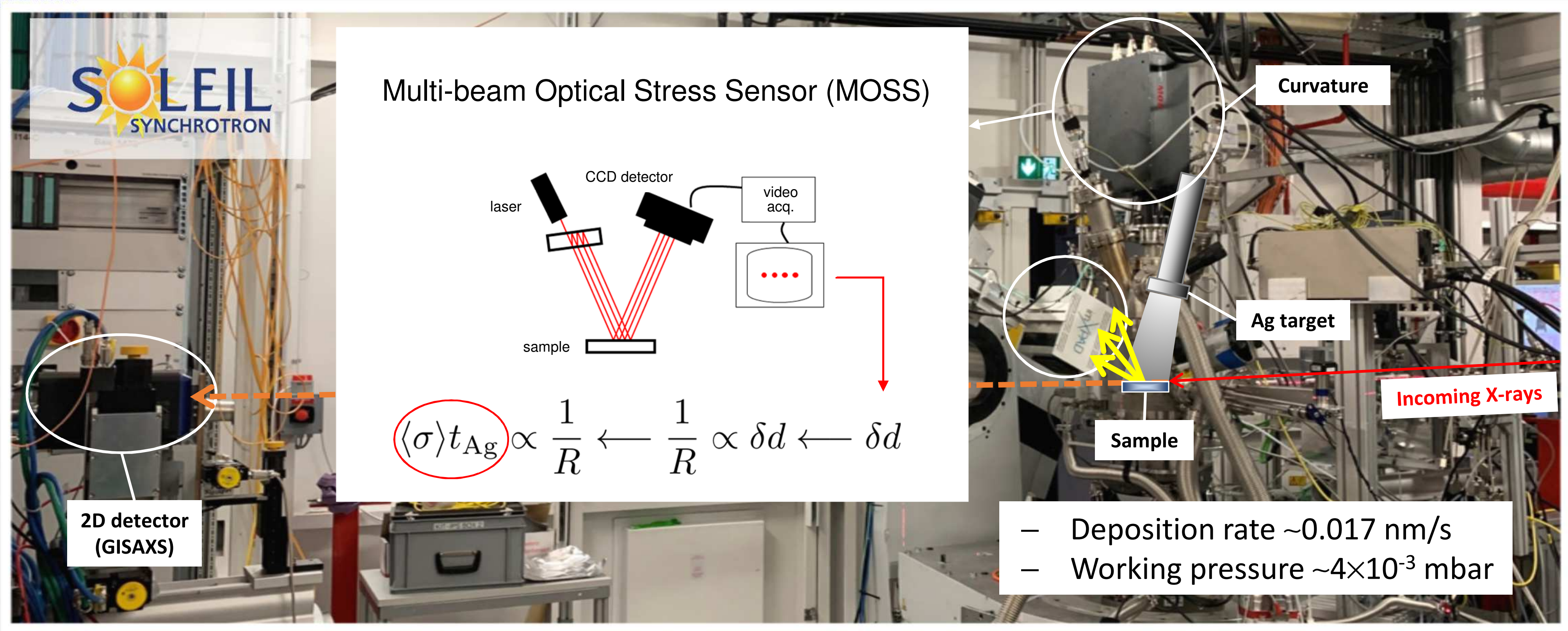

- **Simultaneous measurements during magnetron sputtering Ag deposition on SiO_x/Si**
  - GISAXS: island morphology and organization
  - GID: crystal structure, grain size and orientation…
  - Substrate curvature measurements: stress evolution

In situ and real-time studies of ultrathin silver films

- **GISAXS**
- **GID**
- **Stress**

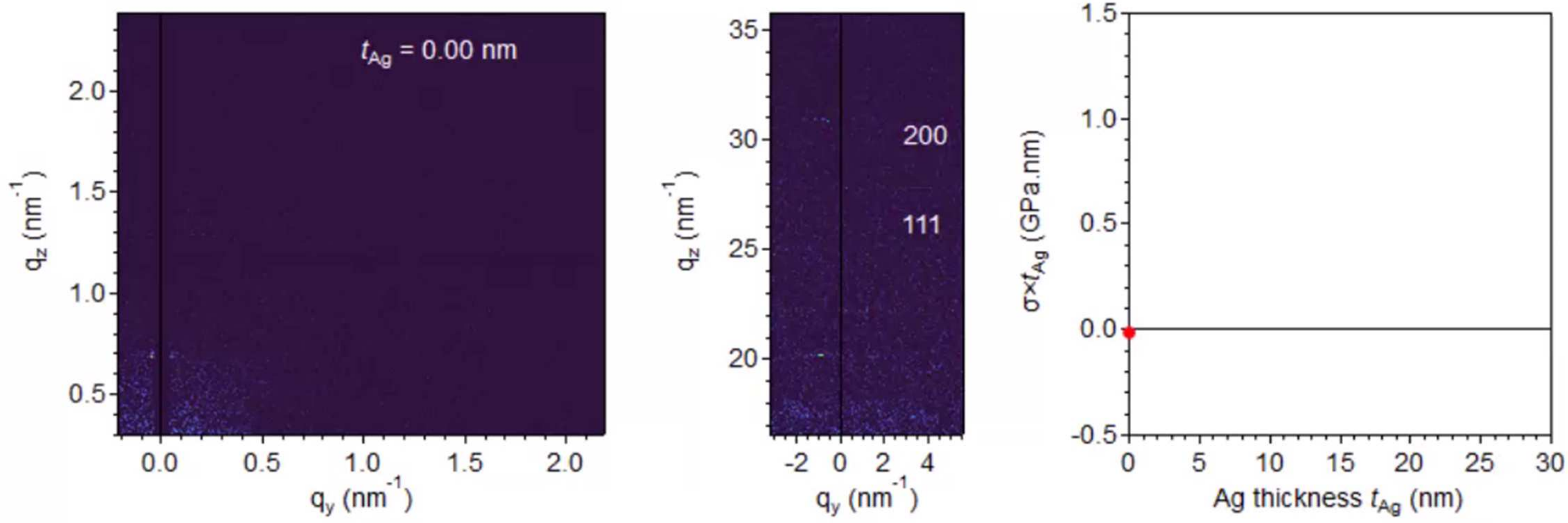

Ag on SiO_x/Si (p_N/p_{tot} = 0)

G. Abadias, A. Michel, K. Solanki (P')
M. Kamiński, B. Krause (KIT)
A. Coati, Y. Garreau, A. Resta, A. Vlad (SOLEIL)

In situ and real-time studies of ultrathin silver films

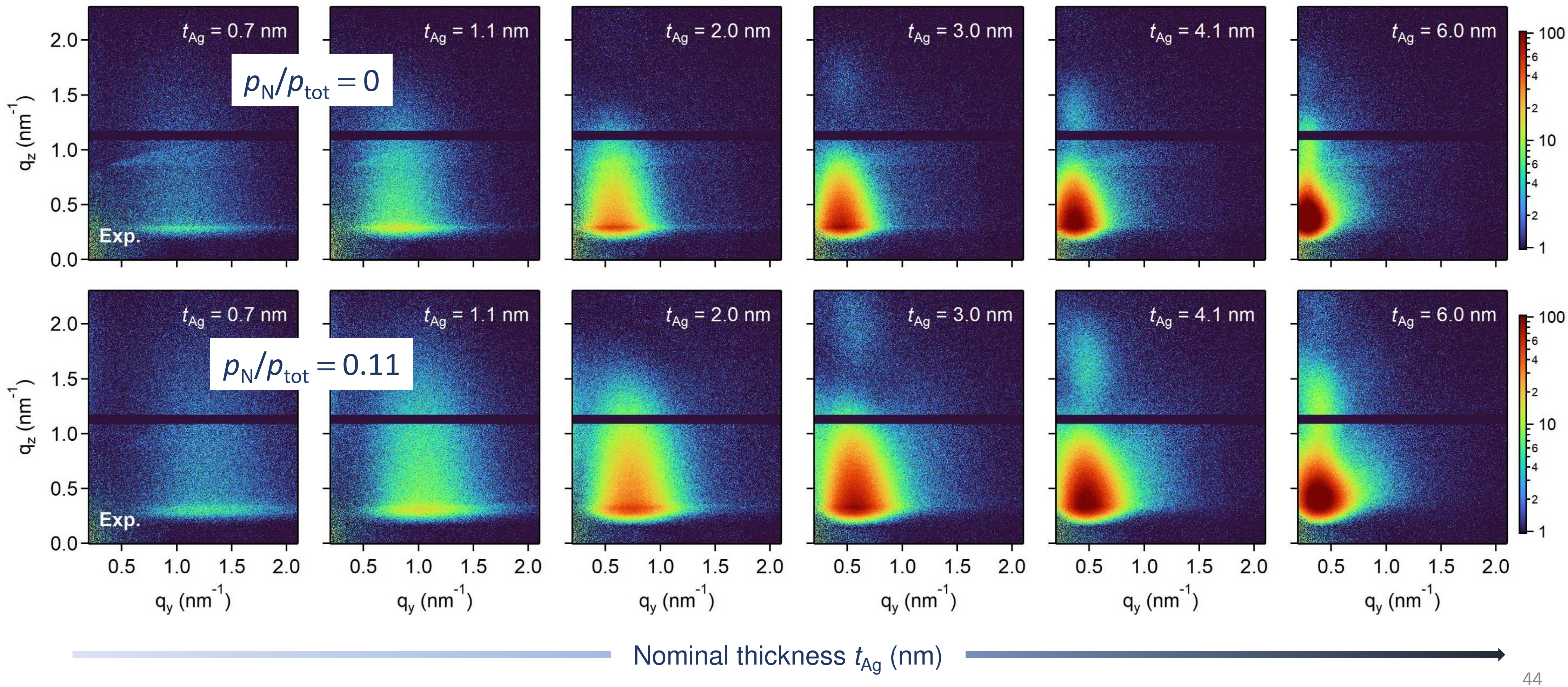

In situ and real-time studies of ultrathin silver films

- **GISAXS**

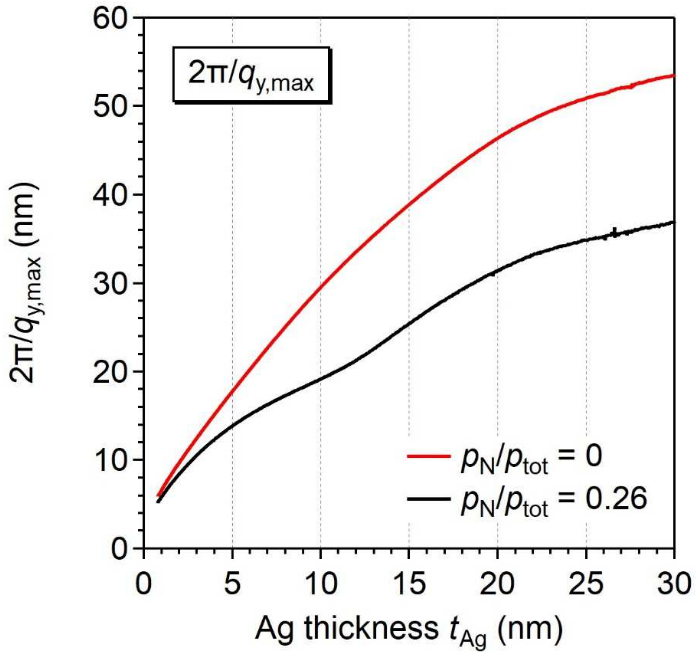

- **GID**

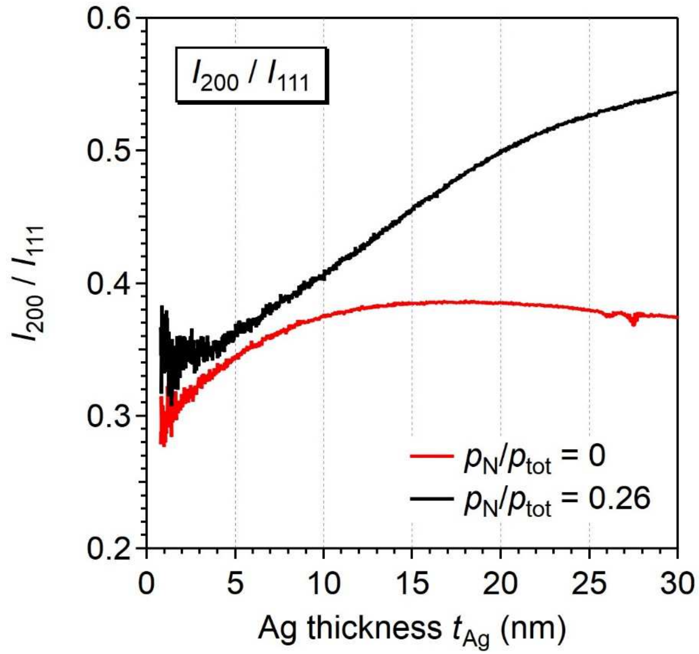

- **Stress**

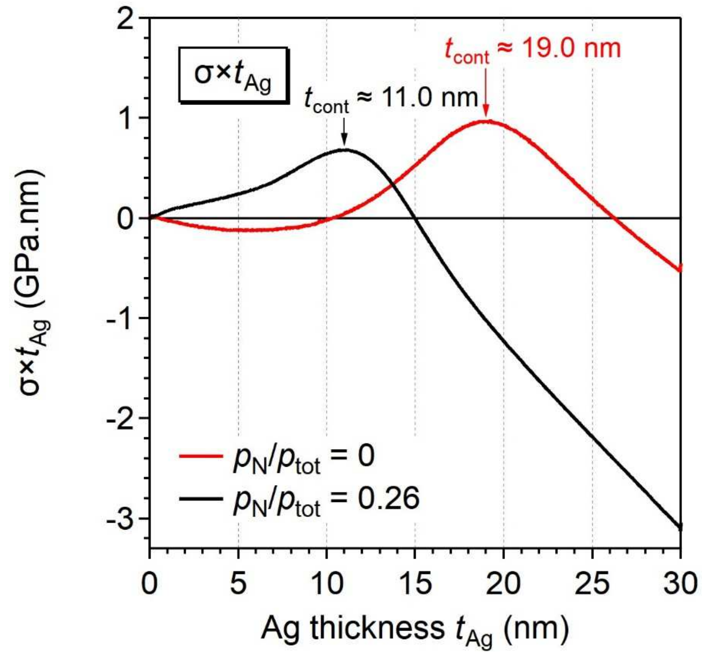

G. Abadias, A. Michel, K. Solanki (P')
M. Kamiński, B. Krause (KIT)
A. Coati, Y. Garreau, A. Resta, A. Vlad (SOLEIL)

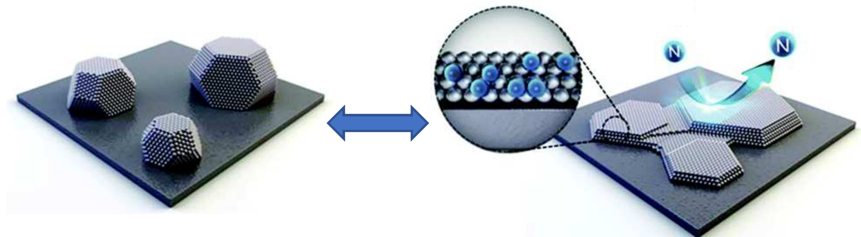

Yun *et al.*, Nanoscale **12** (2020) 1749

Gold NPs in topological defects of smectic films

Coll. E. Lacaze

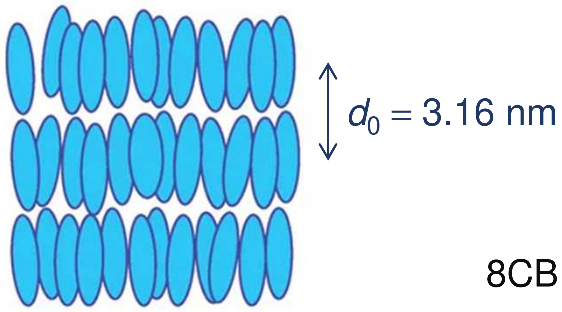

smectic phase

8CB molecule

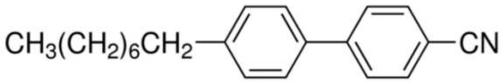

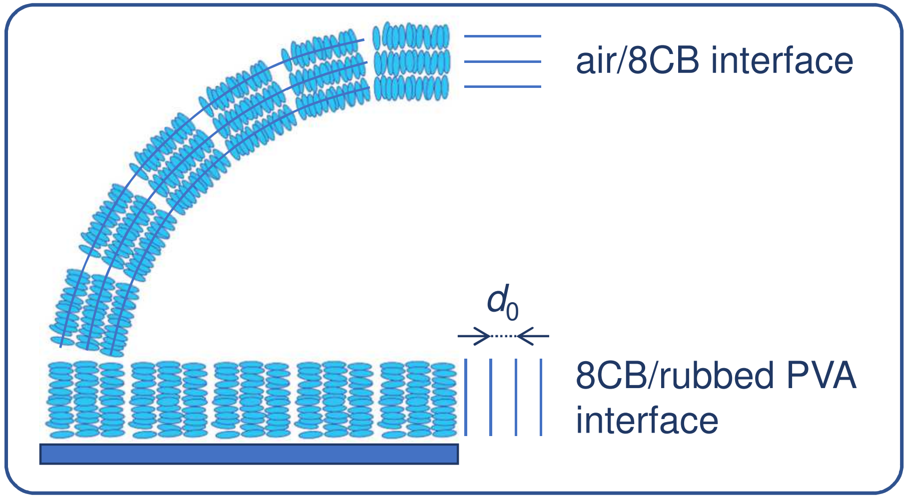

Periodic array of flattened hemicylinders with unidirectional orientation

- Internal structure of the hemicylinders ?
- Self-assembly of gold nanoparticles ?

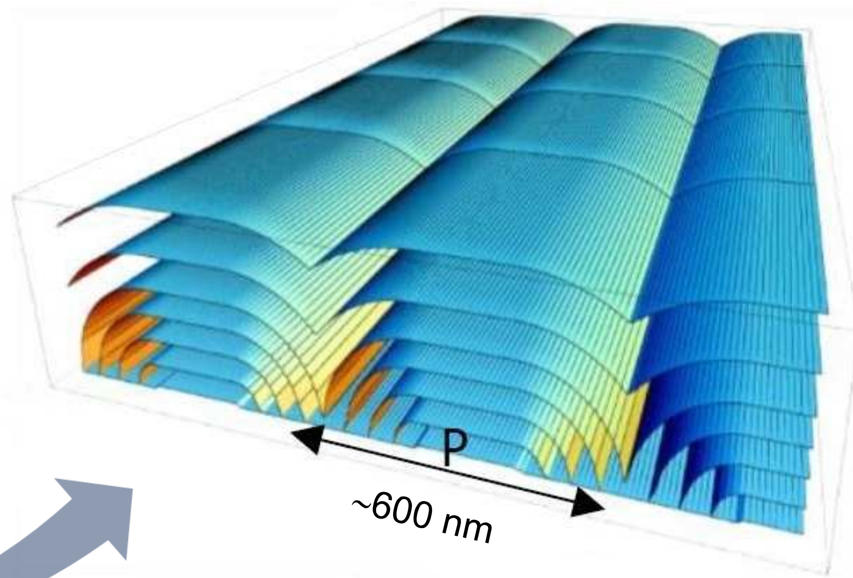

Gold NPs in topological defects of smectic films

Coll. E. Lacaze

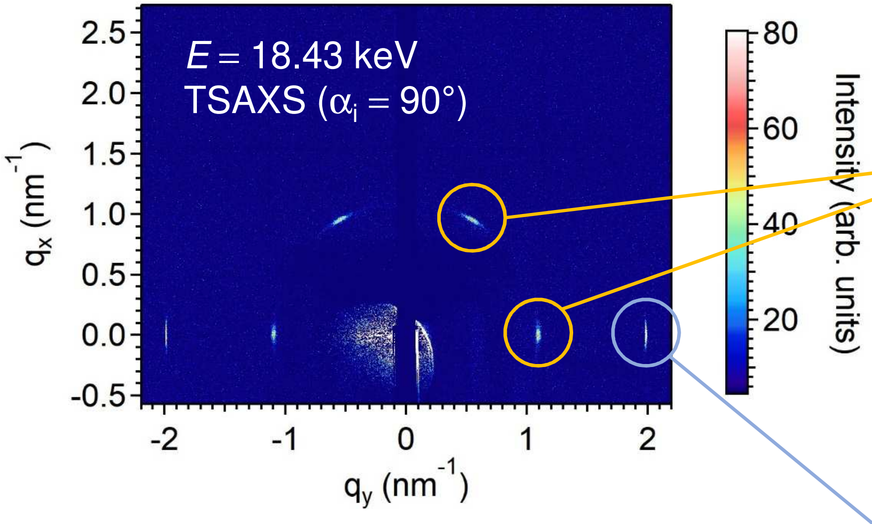

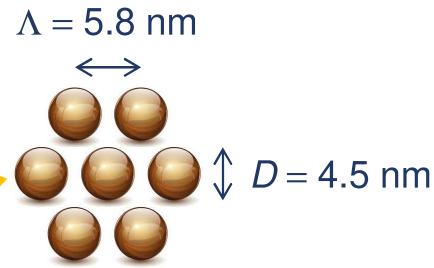

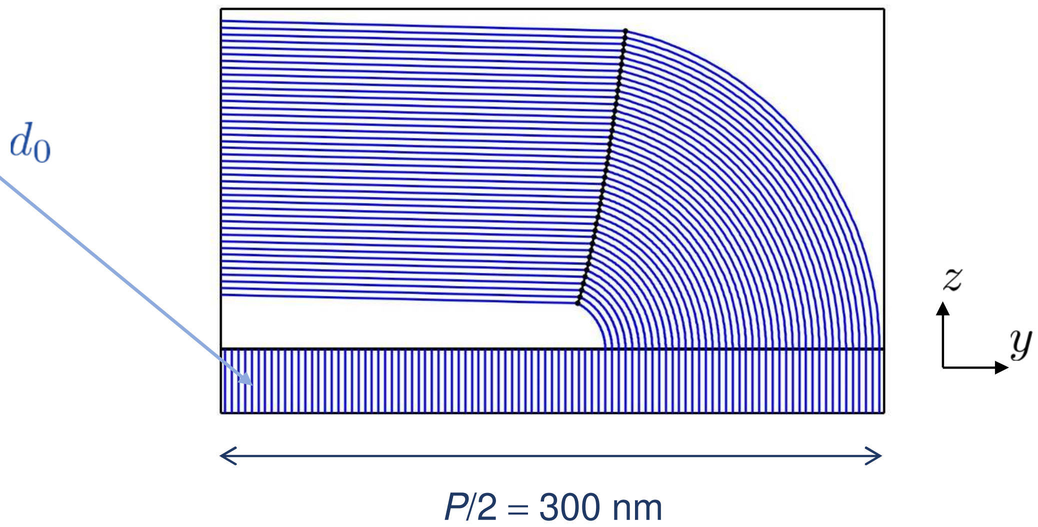

Do *et al.*, Nano Lett. **20** (2020) 1598
Niyonzima *et al.*, Phys. Rev. Lett. (accepted)

Gold NPs in topological defects of smectic films

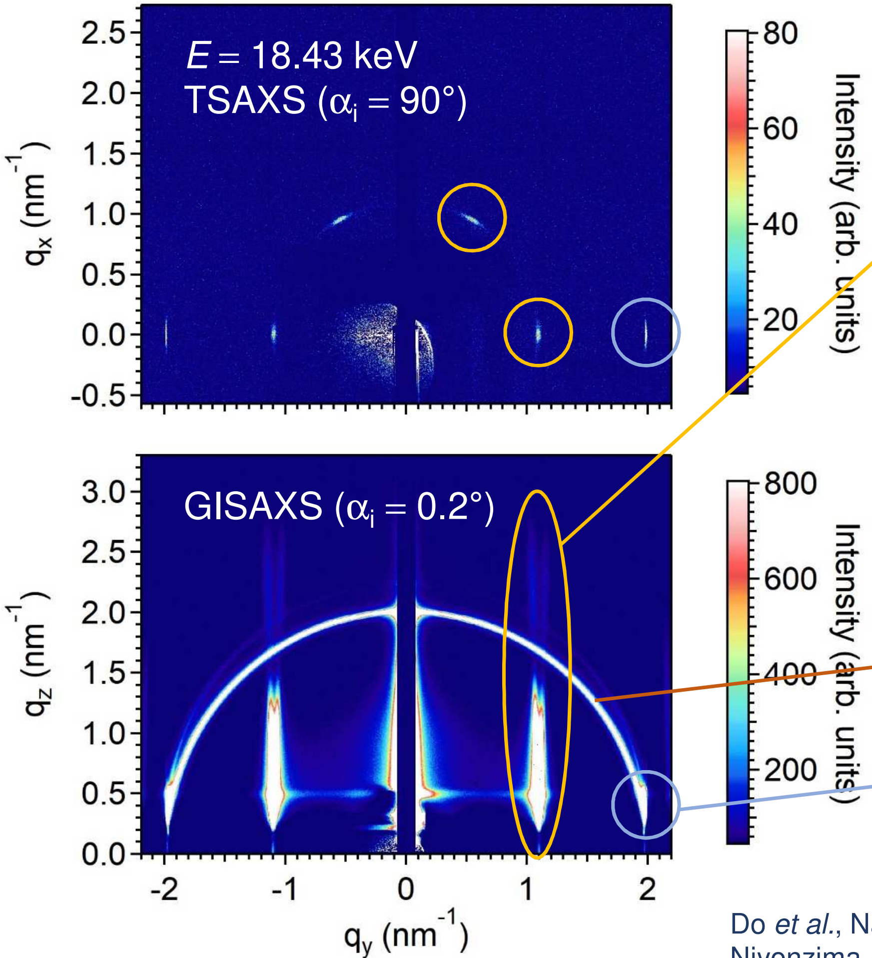

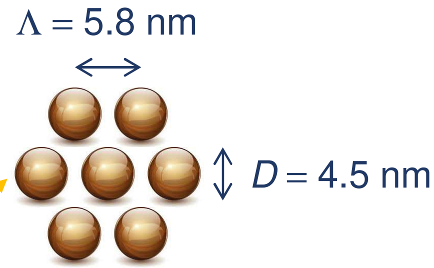

Coll. E. Lacaze

$$d_{N,N+1} = d_0 \left[1 + \frac{1}{N\,(N+1)}\right]$$

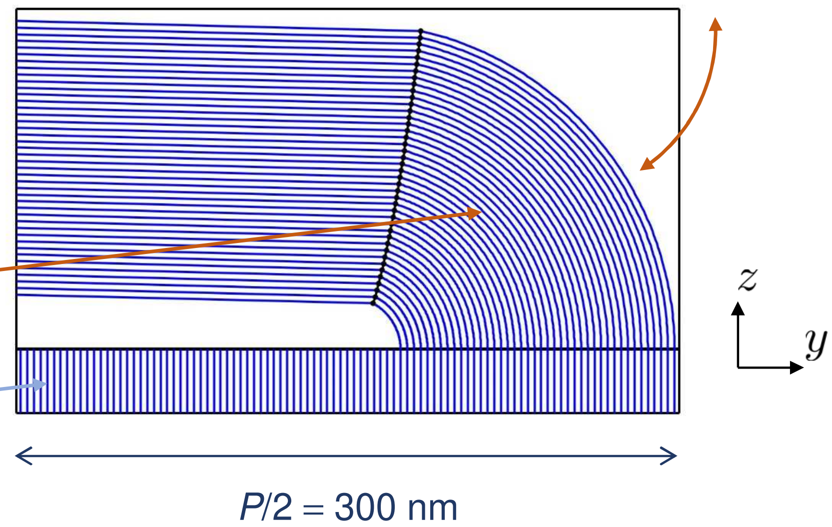

Do *et al.*, Nano Lett. **20** (2020) 1598
Niyonzima *et al.*, Phys. Rev. Lett. (accepted)

Gold NPs in topological defects of smectic films

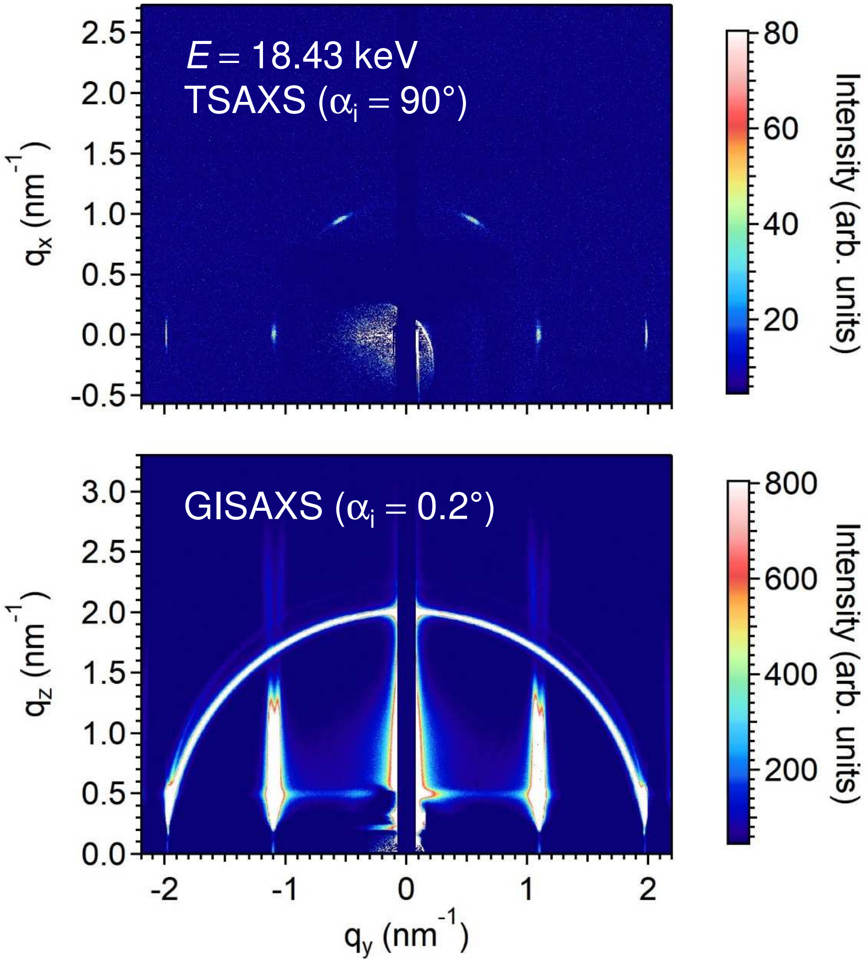

nano-GISAXS
$\alpha_i = 0.6°$ $E = 15$ keV
Beam size ~150 nm
Step ~250 nm

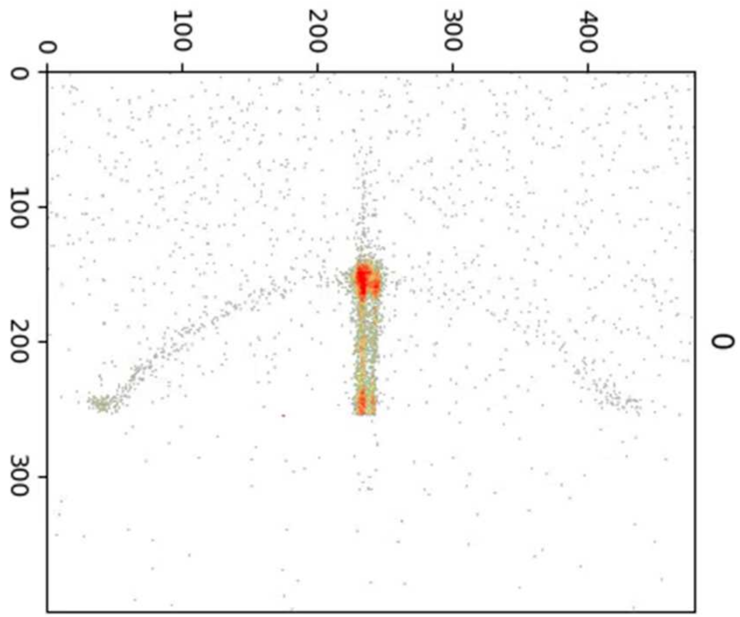

Coll. E. Lacaze

ID13 beamline

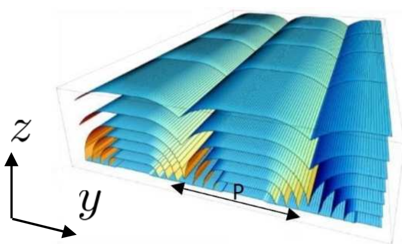

MERCI